Solutions of Chandrasekhar's basic problem in radiative transfer via theory of functional connections

Graphical Abstract

Solutions of Chandrasekhar's Basic Problem in Radiative Transfer via Theory of Functional Connections

Mario De Florio, Enrico Schiassi, Roberto Furfaro, Barry D. Ganapol, Domiziano Mostacci

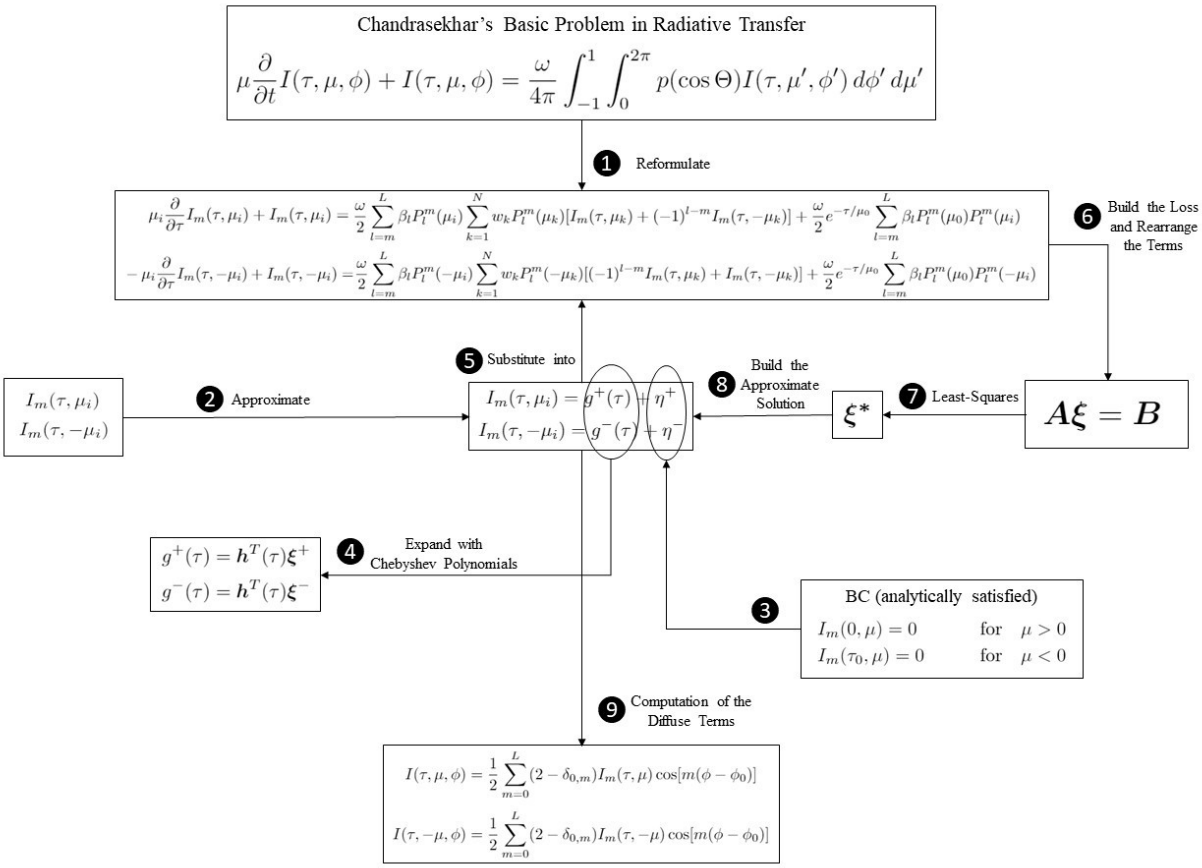

Highlights

Solutions of Chandrasekhar's Basic Problem in Radiative Transfer via Theory of Functional Connections

Mario De Florio, Enrico Schiassi, Roberto Furfaro, Barry D. Ganapol, Domiziano Mostacci

- A highly accurate solution for Chandrasekhar's Basic Problem in Radiative Transfer is proposed
- The forward and backward scattered photon fluxes are computed via Theory of Functional Connections
- The boundary conditions are always analytically satisfied via appropriate constrained expressions
- The boundary-free solution is expanded in Chebyshev polynomials
- The constant coefficients of the Chebyshev polynomials expansion are computed via Least-Squares methods
- Seven digits of accuracy are achieved when compared to the available benchmarks

Solutions of Chandrasekhar's Basic Problem in Radiative Transfer via Theory of Functional Connections

Mario De Florio[a], Enrico Schiassi[a], Roberto Furfaro[a,b,*], Barry D. Ganapol[b], Domiziano Mostacci[c]

[a]*Department of Systems & Industrial Engineering, The University of Arizona, Tucson, AZ, USA*
[b]*Department of Aerospace & Mechanical Engineering, The University of Arizona, Tucson, AZ, USA*
[c]*Laboratorio di Ingegneria Nucleare di Montecuccolino, Alma Mater Studiorum - Università di Bologna, Bologna, Italy*

Abstract

We present a novel approach to solving Chandrasekhar's problem in radiative transfer using the recently developed *Theory of Functional Connections*. The method is designed to elegantly and accurately solve the Linear Boundary Value Problem from the angular discretization of the integrodifferential Boltzmann equation for Radiative Transfer. The proposed algorithm falls under the category of numerical methods for the solution of radiative transfer equations. This new method's accuracy is tested via comparison with the published benchmarks for Mie and Haze L scattering laws.

Keywords:
Transport Theory, Radiative Transfer, Theory of Functional Connections, Mie Scattering, Haze L Problem, Least-Squares

1. Introduction

Radiative transfer theory, i.e. the study of how electromagnetic radiation propagates through a medium, is described by the Radiative Transfer Equation (RTE). The latter mathematically describes how particles moving through a medium are affected by a variety of physical processes, including absorption, scattering and emission. In this work, we consider what is known as Chandrasekhar's basic problem in radiative transfer [1], i.e. the problem of computing the intensity of the photons in a finite slab illuminated by a beam of light incident on one surface.
Historically, several methods have been proposed in the literature to solve the resulting RTE or the integro-differential Boltzmann equation for photons transport. The Discrete Ordinates Method (DOM) has been an effective, purely numerical method of solution available to the transport analysts for nearly 70 years. First proposed by Wick [2] in 1943 and later extensively developed by Chandrasekhar [1], DOM has undergone numerous changes and improvements over the years, with the goal of obtaining more accurate solutions. One of such changes was given by Carlson (1958) [3], who reformulated the DOM by introducing a discretization of the continuous angular variable. This DOM-based approach was named the S_n (S stands for segment, since it uses line segments to approximate the $\mu-$dependence of the angular flux) method and it has been widely employed for many radiative transfer problems [4, 5, 6]. Further methods were subsequently explored. For example, in the C_N method, developed by Benoist and Kavenoky (1968) [7], the angular flux is approximated by an expansion of a complete orthogonal basis, such as a series of Legendre polynomials. The C_N method in turn was further modified by Siewert and Benoist, who developed the F_N method [8] in 1979. F_N was employed to solve the half-space albedo problem and the half-space constant-source problem. Initially used to solve problems in neutron transport theory, it was subsequently applied in several radiative transfer applications [9, 10, 11]. In 1980, Benassi et al. [12] proposed a new P_N method, in which exact particular solutions and the spherical harmonics method [13] were combined to compute the partial heat fluxes for a general class of radiative heat-transfer problems. Siewert and Thomas [14] later in 1989, extended the P_N approximation to the equation of transfer for the case of a general inhomogeneous source term. Finally, at the end of the last millennium (1999), the first version of the Analytical Discrete Ordinates (ADO) method was presented by Barichello and Siewert [15]. Conceived as a modern version of the DOM, the ADO method generated one of the most accurate numerical results for radiative transfer problems [16]. Recently, ADO

*Corresponding author: Roberto Furfaro, robertof@email.arizona.edu

has been extended to solve radiative transfer problems in vegetation [17]. However, research in generating accurate solutions for the basic Chandrasekhar problem and the general RTE continued. In the last decade, Ganapol refined the S_n method in an elegant way, giving life to the Converged S_n method, or CS_n [18]. It is basically an extrapolation of the conventional, fully discretized, S_n solution to near-zero spatial and angular discretization. The distinctiveness of the CS_n method lies in its simplicity, which makes it accessible to those who are not proficient in solving transport equations, while achieving highly accurate solutions. A multi-problem strategy based on S_N acceleration is presented by Picca, Furfaro and Ganapol[19].

All the above mentioned work has shown that in the last 70 years, researchers have developed several methods in order to achieve accurate and efficient numerical solutions for many problems in the radiative transfer field.

In this paper, we propose and develop a novel approach that will open new paths to solve RTEs. The proposed approach applies the *Theory of Functional Connections* (TFC), recently designed and developed by Mortari [20], to solve Chandrasekhar's Basic Problem in Radiative Transfer. TFC was born as a new framework for functional interpolation [20]. It has been successfully applied to solving both linear and non-linear differential equations [21, 22] to machine error accuracy in milliseconds. Moreover the authors have successfully applied TFC to space guidance problems like Energy and Fuel Optimal Landing on large and small planetary bodies [23, 24, 25].
The method transforms ODEs with boundary and/or initial conditions into unconstrained optimization problems, which are solved via least-square (or iterative least-square for the non-linear case), by embedding the conditions into a constrained expression containing the ICs/BCs and a freely chosen function. Such an expression can be expressed in the following general form [20]:

$$y(t) = g(t) + \sum_{k=1}^{n} \eta_k p_k(t) = g(t) + \boldsymbol{\eta}^T \mathbf{p}(t) \tag{1}$$

Eq. (1) is called *constrained expression* (CE). The $p_k(t)$ are n assigned linearly independent functions and the $g(t)$ is a free function, which must be linearly independent from the $p_k(t)$ functions. The values of the η_k parameters are calculated by imposing the set of n linear constraints in $y(t)$. By doing so, the constraints for the differential equations are satisfied for any chosen $g(t)$. So far, it has been demonstrated that TFC method in solving ODEs has the best performance when $g(t)$ is selected as an expansion of basis function such as the Chebyshev orthogonal polynomials [21]. That is:

$$g(t) = \sum_{i=0}^{m_{op}-1} h_i(x)\xi_i = \mathbf{h}^T(t)\boldsymbol{\xi} \tag{2}$$

where the polynomial constant coefficients ξ are the unknown to be computed, $h_i(x)$ is the i_{th} orthogonal polynomial, and m_{op} is the number of basis considered. By substituting the CE in the ODE, for linear problems as the one tackled in this paper, we will obtain a linear system of the type $A\xi = b$ to be computed via LS to find the solution $y(t)$.
Here, we propose to extend the TFC framework to solve RTEs. Starting from Chandrasekhar's Basic RTE and applying an angular discretization as in [16], the basic integrodifferential Boltzmann equation is transformed into a system of ODEs. The latter is cast as a Linear Boundary Value Problem (BVP) that is solved via the TFC method. Constrained expressions are generated and the resulting free-function is expanded in the basis of Chebyshev orthogonal polynomials. Such expansion ultimately results in a linear system that is solved via a Least-Square algorithm. Most importantly, the proposed method is shown to be elegant, concise, versatile and yields a straightforward numerical implementation.

The paper is organized as follows. In section 2 a summary of the TFC methodology is reported together with an example of methodological application of the RTE to the simple Two-Stream Approximation. In section 3, the basic Chandrasekhar RTE is stated and formulated. In sections 4 and 5, the new TFC-based numerical algorithm is detailed. Finally, numerical results are presented and discussed in section 6.

2. TFC Approach to Solving ODE Boundary Value Problems

2.1. Method

For the convenience of the reader, how the TFC method works to tackle generic linear and non-linear ODEs is summarized in Fig. 1, and following, we give a simple example of the application of TFC to solving

the class of BVPs. The detailed derivation can be found in [21, 22]. Consider solving a first-order boundary value problem such that:

$$F(\tau, y, \dot{y}) = 0 \quad \text{subject to:} \quad y(\tau_0) = y_0. \tag{3}$$

The CE is built from Eq. (1) by setting $p_1(\tau) = 1$ (see ref. [21, 22] for the details of this decision):

$$y(\tau) = g(\tau) + \eta \tag{4}$$

By applying the constraint, we get:

$$y(\tau_0) = y_0 = g_0 + \eta; \qquad \Longrightarrow \qquad \eta_1 = y_0 - g_0$$

which is plugged into Eq. (4) to obtain at the final CE:

$$y(\tau) = g(\tau) + (y_0 - g_0) \tag{5}$$

which represents all possible functions satisfying the boundary value constraint. The derivative then follows:

$$\dot{y}(\tau) = \dot{g}(\tau). \tag{6}$$

By substituting Eq. (5) and Eq. (6) into the Eq. (3), the original differential equation is transformed into a new differential equation $\tilde{F}$, which now is boundary free, and it is only a function of the independent variable τ and the free-function $g(\tau)$, that is:

$$\tilde{F}\left(\tau, g, \dot{g}\right) = 0.$$

This differential equation is now *unconstrained* and will always satisfy the boundary-value due to the way Eq. (4) is built. In order to solve this problem numerically, we define the function $g(\tau)$ as an expansion of some known basis with unknown constant coefficients such that:

$$g(\tau) = \boldsymbol{h}(\tau)^T \boldsymbol{\xi} \tag{7}$$

where $\boldsymbol{\xi}$ is a $m_{op} \times 1$ vector of unknown constant coefficients where m_{op} is the number of basis functions used. In general, the basis functions are defined on an inconsistent domain $x \in [x_0, x_f]$ (Chebyshev polynomials are defined on $x \in [-1, +1]$, Fourier series is defined on $x \in [-\pi, +\pi]$, etc.). Thus, these functions must be linearly mapped to the independent variable τ. This can be done using the following linear transformation:

$$x = x_0 + \frac{x_f - x_0}{t_f - t_0}(\tau - \tau_0) \quad \leftrightarrow \quad \tau = \tau_0 + \frac{\tau_f - \tau_0}{x_f - x_0}(x - x_0).$$

where $\tau \in [\tau_0, \tau_f]$.
Defining:

$$c = \frac{x_f - x_0}{\tau_f - \tau_0} \tag{8}$$

by the derivative chain rule, the derivative of Eq. (7) is,

$$\frac{\mathrm{d}g(\tau)}{\mathrm{d}\tau} = c\,\boldsymbol{\xi}^T \frac{\mathrm{d}\boldsymbol{h}(x)}{\mathrm{d}x},$$

which defines all mappings of the free-function. Finally, the domain τ must be discretized by M points. In this paper, we consider $g(\tau)$ as an expansion of Chebyshev polynomials. By defining the free function in this way and then discretizing the domain of the differential equations, $\tilde{F}$ becomes:

$$\tilde{F}(\boldsymbol{\xi}) = 0,$$

which is now a function (linear or nonlinear) of only the unknown coefficients $\boldsymbol{\xi}$. Eq. (2.1) is now an *unconstrained* optimization problem that can be solved via different optimization schemes. In this paper, as we deal with a linear problem, we use a linear LS to solve for the unknown coefficients $\boldsymbol{\xi}$.

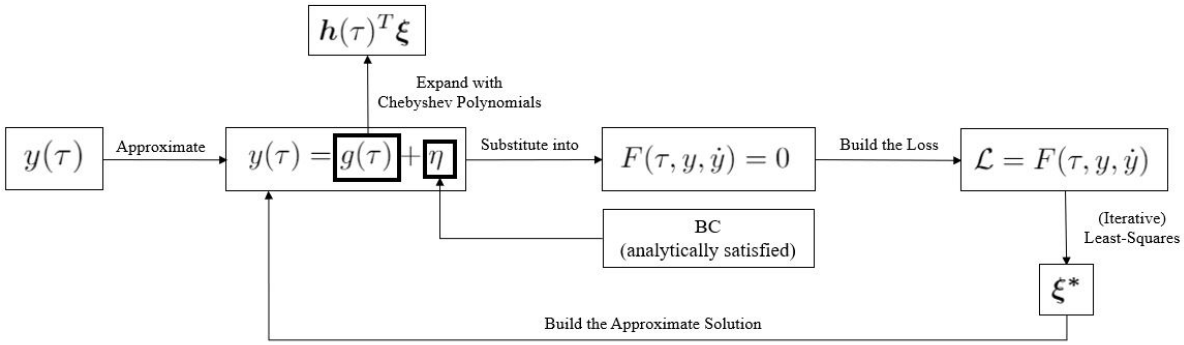

Figure 1: Schematic of the general TFC framework to solve linear and non-linear ODEs with one constraint in one point.

2.2. Example: Radiative Transfer Problem with Two-Stream Approximation

This example shows how to apply the TFC method to solve a simple system of ODEs. The system is the following:

$$\mu\frac{dy_1}{d\tau} + y_1(\tau) = \frac{\omega}{2}\left[y_1(\tau) + y_2(\tau)\right] + \frac{\omega}{2}S_0 e^{-\frac{\tau}{\mu_0}} \tag{9}$$

$$-\mu\frac{dy_2}{d\tau} + y_2(\tau) = \frac{\omega}{2}\left[y_2(\tau) + y_1(\tau)\right] + \frac{\omega}{2}S_0 e^{-\frac{\tau}{\mu_0}}, \tag{10}$$

subject to,

$$y_1(0) = 0 \tag{11}$$

$$y_2(\tau_0) = 0 \tag{12}$$

that represents an isotropic scattering radiative transfer equation with two-stream approximation [26], arising from Chandrasekhar [1], explained in details in the next section. The solutions of this system of ODEs represent the trend of scattered photons (forward and backward) through a mono-dimensional slab of thickness τ_0. For this example,the following parameters are used:

- $\mu = 0.5$ is the cosine of the polar angle
- $\mu_0 = 0.8$ is the cosine of incident beam angle
- $\tau_0 = 1$ is the optical thickness
- $\omega = 0.9$ is the single scattering albedo
- $S_0 = 1$ is the source intensity

The detailed explanation of these parameters physically represent will be given in the next section. The unknowns are $y_1(\tau)$ and $y_2(\tau)$ that represent the forward and backward scattered photons fluxes respectively. The first step of the TFC framework is to build the constrained expressions (CE) for the unknowns. According to previous explanation, the CEs are:

$$y_1(\tau) = \left(\boldsymbol{h} - \boldsymbol{h}_0\right)^T\boldsymbol{\xi}_1 \tag{13}$$

$$y_2(\tau) = \left(\boldsymbol{h} - \boldsymbol{h}_f\right)^T\boldsymbol{\xi}_2 \tag{14}$$

where $\boldsymbol{h}$ are the Chebyshev polynomials, and $\boldsymbol{h}_0$ and $\boldsymbol{h}_f$ are the Chebyshev polynomials computed at $\tau = 0$ and $\tau = \tau_0$, respectively.
The derivatives of the CEs are:

$$\frac{dy_1}{d\tau} = c\,\boldsymbol{h}'^T\boldsymbol{\xi}_1 \tag{15}$$

$$\frac{dy_2}{d\tau} = c\,\boldsymbol{h}'^T\boldsymbol{\xi}_2 \tag{16}$$

where $\boldsymbol{h}'$ are the derivatives of $\boldsymbol{h}$ with respect to the variable x, and c is the mapping coefficient from τ to x (and vice-versa) as defined in Eq. (8).
By plugging the CEs and their derivatives into the system of ODEs, we get the following:

$$\mu\, c\, \boldsymbol{h}'\boldsymbol{\xi}_1 + (\boldsymbol{h}-\boldsymbol{h}_0)^T\, \boldsymbol{\xi}_1 = \frac{\omega}{2}\left[(\boldsymbol{h}-\boldsymbol{h}_0)^T\, \boldsymbol{\xi}_1 + (\boldsymbol{h}-\boldsymbol{h}_f)^T\, \boldsymbol{\xi}_2\right] + \frac{\omega}{2} S_0 e^{-\frac{\tau}{\mu_0}} \tag{17}$$

$$-\mu\, c\, \boldsymbol{h}'\boldsymbol{\xi}_2 + (\boldsymbol{h}-\boldsymbol{h}_f)^T\, \boldsymbol{\xi}_2 = \frac{\omega}{2}\left[(\boldsymbol{h}-\boldsymbol{h}_f)^T\, \boldsymbol{\xi}_2 + (\boldsymbol{h}-\boldsymbol{h}_0)^T\, \boldsymbol{\xi}_1\right] + \frac{\omega}{2} S_0 e^{-\frac{\tau}{\mu_0}}, \tag{18}$$

The losses are:

$$\mathcal{L}_1 = \mu\, c\, \boldsymbol{h}'\boldsymbol{\xi}_1 + (\boldsymbol{h}-\boldsymbol{h}_0)^T\, \boldsymbol{\xi}_1 - \frac{\omega}{2}\left[(\boldsymbol{h}-\boldsymbol{h}_0)^T\, \boldsymbol{\xi}_1 + (\boldsymbol{h}-\boldsymbol{h}_f)^T\, \boldsymbol{\xi}_2\right] - \frac{\omega}{2} S_0 e^{-\frac{\tau}{\mu_0}} \tag{19}$$

$$\mathcal{L}_2 = -\mu\, c\, \boldsymbol{h}'\boldsymbol{\xi}_2 + (\boldsymbol{h}-\boldsymbol{h}_f)^T\, \boldsymbol{\xi}_2 - \frac{\omega}{2}\left[(\boldsymbol{h}-\boldsymbol{h}_f)^T\, \boldsymbol{\xi}_2 + (\boldsymbol{h}-\boldsymbol{h}_0)^T\, \boldsymbol{\xi}_1\right] - \frac{\omega}{2} S_0 e^{-\frac{\tau}{\mu_0}} \tag{20}$$

As the problem is linear, by imposing the losses to be equal zero and re-arranging the terms we get the following system of linear algebraic equations:

$$\left[\mu\, c\, \boldsymbol{h}' + (\boldsymbol{h}-\boldsymbol{h}_0) - \frac{\omega}{2}(\boldsymbol{h}-\boldsymbol{h}_0)\right]^T \boldsymbol{\xi}_1 - \left[\frac{\omega}{2}(\boldsymbol{h}-\boldsymbol{h}_f)^T\right] \boldsymbol{\xi}_2 = \frac{\omega}{2} S_0 e^{-\frac{\tau}{\mu_0}} \tag{21}$$

$$\left[-\frac{\omega}{2}(\boldsymbol{h}-\boldsymbol{h}_0)^T\right] \boldsymbol{\xi}_1 + \left[-\mu\, c\, \boldsymbol{h}' + (\boldsymbol{h}-\boldsymbol{h}_f) - \frac{\omega}{2}(\boldsymbol{h}-\boldsymbol{h}_f)\right]^T \boldsymbol{\xi}_2 = \frac{\omega}{2} S_0 e^{-\frac{\tau}{\mu_0}} \tag{22}$$

In matrix form the system becomes:

$$\underbrace{\begin{bmatrix} \mu c\, \boldsymbol{h}'^T + (\boldsymbol{h}-\boldsymbol{h}_0)^T - \frac{\omega}{2}(\boldsymbol{h}-\boldsymbol{h}_0)^T & -\frac{\omega}{2}(\boldsymbol{h}-\boldsymbol{h}_f)^T \\ -\frac{\omega}{2}(\boldsymbol{h}-\boldsymbol{h}_0)^T & -\mu c\, \boldsymbol{h}'^T + (\boldsymbol{h}-\boldsymbol{h}_f)^T - \frac{\omega}{2}(\boldsymbol{h}-\boldsymbol{h}_f)^T \end{bmatrix}}_{A} \underbrace{\begin{bmatrix} \boldsymbol{\xi}_1 \\ \boldsymbol{\xi}_2 \end{bmatrix}}_{\xi} = \underbrace{\begin{bmatrix} \frac{\omega}{2} S_0 e^{-\frac{\tau}{\mu_0}} \\ \frac{\omega}{2} S_0 e^{-\frac{\tau}{\mu_0}} \end{bmatrix}}_{b} \tag{23}$$

As the problem is linear, we can solve for $\boldsymbol{\xi}$ using a least-squares. That is:

$$\boldsymbol{\xi} = \left(A^T A\right)^{-1} A^T b \tag{24}$$

Once $\boldsymbol{\xi}$ are computed, the final solutions are built by plugging $\boldsymbol{\xi}$ into the CEs (13), as shown in Fig. 1.
The results are reported in Tables 1 and 2, where they are compared to the results computed according to the ADO method. As we can see, the boundary conditions are analytically satisfied.

Slab Points	ADO	TFC
0	$1.110223024625157 \times 10^{-16}$	0
0.1	0.121476763490043	0.121476763490043
0.2	0.217584323416591	0.217584323416591
0.3	0.291745312795815	0.291745312795815
0.4	0.346937565918151	0.346937565918151
0.5	0.385747980285517	0.385747980285517
0.6	0.410419885421222	0.410419885421222
0.7	0.422894687247150	0.422894687247150
0.8	0.424848465764781	0.424848465764781
0.9	0.417724123526887	0.417724123526887
1	0.402759611584474	0.402759611584474

Table 1: ADO and TFC forward scattered flux y_1. The latter is obtained with $M = 100$ and $m_{op} = 40$. M is the number of discretization points on τ and m_{op} is the number of basis used.

Slab Points	ADO	TFC
0	0.504726885720671	0.504726885720671
0.1	0.467993882643466	0.467993882643466
0.2	0.427166877800790	0.427166877800790
0.3	0.382783602872154	0.382783602872154
0.4	0.335285178981115	0.335285178981115
0.5	0.285027561759344	0.285027561759344
0.6	0.232291508206183	0.232291508206183
0.7	0.177291238875862	0.177291238875862
0.8	0.120181947999640	0.120181947999640
0.9	0.061066295681211	0.061066295681211
1	$-5.551115123125783 \times 10^{-17}$	0

Table 2: ADO and TFC backward scattered flux y_2. The latter is obtained with $M = 100$ and $m_{op} = 40$.

3. Radiative Transfer Equation: Problem formulation

As we previously mentioned, we consider Chandrasekhar's basic problem for Radiative Transfer for an incoming beam at $x = 0$, as shown in Fig. 2, following the notation used in [27, 16] the radiative transfer equation is written as:

$$\mu \frac{\partial}{\partial \tau} I(\tau, \mu, \phi) + I(\tau, \mu, \phi) = \frac{\omega}{4\pi} \int_{-1}^{1} \int_{0}^{2\pi} p(\cos\Theta) I(\tau, \mu', \phi')\, d\phi'\, d\mu' \tag{25}$$

where Θ is the scattering angle, $\mu \in [-1, 1]$ is the cosine of the polar angle , $\tau \in [0, \tau_0]$ is the optical variable, τ_0 is the optical thickness, $\phi \in [0, 2\pi]$ is the azimuthal angle, and $\omega \in [0, 1]$ is the single scattering albedo.

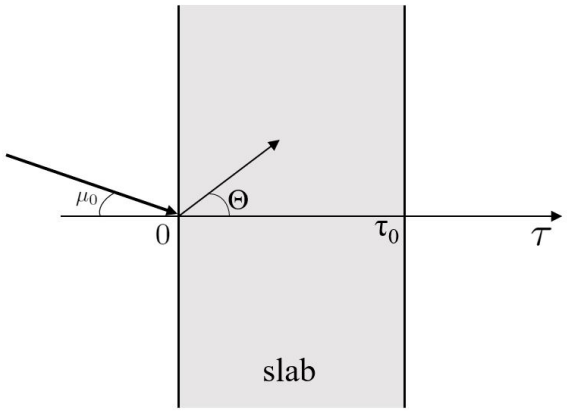

Figure 2: Geometry of the 1D slab for the considered Radiative Transfer Problem.

According to [28], we use the addition theorem to express the phase function in terms of Legendre polynomials:

$$p(\cos\Theta) = \sum_{l=0}^{L} \beta_l P_l(\cos\Theta) \tag{26}$$

where the β_l are the Legendre coefficients in the L^{th} order expansion of scattering law.
The problem is subject to the following constraints/boundary conditions:

$$\begin{cases} I(0, \mu, \phi) = S_0 \pi \delta(\mu - \mu_0)\delta(\phi - \phi_0) & \text{for} \quad \mu > 0 \\ I(\tau_0, \mu, \phi) = 0 & \text{for} \quad \mu < 0 \end{cases} \tag{27}$$

where $S_0\pi$ represents the flux carried by a source beam across a plane normal to the direction of incidence, and μ_0 and ϕ_0 determine the inclination of the source beam.
The solution is defined as the sum of collided (or diffuse) term and uncollided term [16]:

$$I(\tau,\mu,\phi) = I^*(\tau,\mu,\phi) + I^o(\tau,\mu,\phi), \tag{28}$$

where the superscript * refers to the collided beam, and the superscript ^{o} refers to the uncollided beam. The problem is therefore split into two parts. The uncollided term solves the following first order PDE:

$$\mu\frac{\partial}{\partial\tau}I^o(\tau,\mu,\phi) + I^o(\tau,\mu,\phi) = 0 \tag{29}$$

subject to:

$$\begin{cases} I^o(0,\mu,\phi) = S_0\pi\delta(\mu-\mu_0)\delta(\phi-\phi_0) & \text{for} \quad \mu > 0 \\ I^o(0,\mu,\phi) = 0 & \text{for} \quad \mu < 0 \end{cases} \tag{30}$$

where $\mu \in (0,1]$.
The problem (29)-(30) has the following analytical solutions:

$$\begin{cases} I^o(\tau,\mu,\phi) = S_0\pi\delta(\mu-\mu_0)\delta(\phi-\phi_0)e^{-\tau/\mu} & \text{for} \quad \mu > 0 \\ I^o(\tau,\mu,\phi) = 0 & \text{for} \quad \mu < 0 \end{cases} \tag{31}$$

Plugging into the equation (28), we obtain the following:

$$I(\tau,\mu,\phi) = I^*(\tau,\mu,\phi) + S_0\pi\delta(\mu-\mu_0)\delta(\phi-\phi_0)e^{-\tau/\mu} \tag{32}$$

The relation of the phase function and the scattering angle can be expressed using the *Addition Theorem of the Spherical Harmonics* [28]:

$$p(\cos\Theta) = \sum_{m=0}^{L}(2-\delta_{0,m})\sum_{l=m}^{L}\beta_l P_l^m(\mu')P_l^m(\mu)\cos[m(\phi'-\phi)] \tag{33}$$

where the following expression is used to denote the normalized function [29, 30]:

$$P_l^m(\mu) = \left[\frac{(l-m)!}{(l+m)!}\right](1-\mu^2)^{m/2}\frac{d^m}{d\mu^m}P_l(\mu) \tag{34}$$

Thus, we can express the diffuse component as a Fourier expansion with L terms. That is:

$$I^*(\tau,\mu,\phi) = \frac{1}{2}\sum_{m=0}^{L}(2-\delta_{0,m})I_m(\tau,\mu)\cos[m(\phi-\phi_0)] \tag{35}$$

The m^{th} Fourier component satisfies the following linear integro - 1^{st} order PDE:

$$\mu\frac{\partial}{\partial t}I_m(\tau,\mu) + I_m(\tau,\mu) = \frac{\omega}{2}\sum_{l=m}^{L}\beta_l P_l^m(\mu)\int_{-1}^{1}P_l^m(\mu')I_m(\tau,\mu')d\mu' + Q^m(\tau,\mu), \tag{36}$$

where Q is the inhomogeneous source term [16]:

$$Q^m(\tau,\mu) = \frac{\omega}{2}e^{-\tau/\mu_0}\sum_{l=m}^{L}\beta_l P_l^m(\mu_0)P_l^m(\mu) \tag{37}$$

Thus, the problem to solve is the following:

$$\mu\frac{\partial}{\partial t}I_m(\tau,\mu) + I_m(\tau,\mu) = \frac{\omega}{2}\sum_{l=m}^{L}\beta_l P_l^m(\mu)\int_{-1}^{1}P_l^m(\mu')I_m(\tau,\mu')d\mu' + \frac{\omega}{2}e^{-\tau/\mu_0}\sum_{l=m}^{L}\beta_l P_l^m(\mu_0)P_l^m(\mu) \tag{38}$$

Subject to:

$$\begin{cases} I_m(0,\mu) = 0 & \text{for} \quad \mu > 0 \\ I_m(\tau_0,\mu) = 0 & \text{for} \quad \mu < 0 \end{cases} \tag{39}$$

Via discretizing the angle μ into N points in the interval $(0,1]$ according to the Gauss-Legendre quadrature scheme:

$$\mu \quad \longrightarrow \quad \mu = \{\mu_i\}_{i=1}^{N}$$

it follows that:

$$I_m(\tau,\mu) \quad \longrightarrow \quad \mathbf{I}_m(\tau) = \{I_m(\tau,\mu_i)\}_{i=1}^{N} \tag{40}$$

Following the notation used by Siewert [16], suppressing some of the m indexes, and splitting the problem into two equations, for positive and negative values of μ, we get the following set of equations:

$$\begin{aligned} &\mu_i \frac{\partial}{\partial\tau} I_m(\tau,\mu_i) + I_m(\tau,\mu_i) = \\ &= \frac{\omega}{2} \sum_{l=m}^{L} \beta_l P_l^m(\mu_i) \sum_{k=1}^{N} w_k P_l^m(\mu_k)[I_m(\tau,\mu_k) + (-1)^{l-m} I_m(\tau,-\mu_k)] + \frac{\omega}{2} e^{-\tau/\mu_0} \sum_{l=m}^{L} \beta_l P_l^m(\mu_0) P_l^m(\mu_i) \end{aligned} \tag{41}$$

$$\begin{aligned} &-\mu_i \frac{\partial}{\partial\tau} I_m(\tau,-\mu_i) + I_m(\tau,-\mu_i) = \\ &= \frac{\omega}{2} \sum_{l=m}^{L} \beta_l P_l^m(-\mu_i) \sum_{k=1}^{N} w_k P_l^m(-\mu_k)[(-1)^{l-m} I_m(\tau,\mu_k) + I_m(\tau,-\mu_k)] + \frac{\omega}{2} e^{-\tau/\mu_0} \sum_{l=m}^{L} \beta_l P_l^m(\mu_0) P_l^m(-\mu_i) \end{aligned} \tag{42}$$

where the Gauss-Legendre quadrature rule is used to evaluate the integral in the range $[0,1]$.
Equations (41)-(42) with the constraints (39) are a set of N linear first-order ODEs that we will solve via TFC.

4. TFC Formulation of the Problem

In our case, we assume to have one constraint in one point; hence, according to (1), $y(\tau)$ can be expressed as following:

$$y(\tau) = g(\tau) + \eta p(\tau) \tag{43}$$

We set $p(\tau) = 1$, as suggested by [21], and the function $g(\tau)$ as an expansion of Chebyshev polynomials as follows:

$$g(\tau) = \boldsymbol{h}^T(\tau)\boldsymbol{\xi} \tag{44}$$

Since Chebyshev Polynomials are used as basis functions, we need to define a new variable x that ranges in $[-1,1]$. The new x variable is defined as $x = c\tau - 1$, where c is the mapping coefficient:

$$c = \frac{x_f - x_0}{\tau_f - \tau_0}$$

Considering the new independent variable, we have:

$$\begin{cases} I_m(\tau,\mu) = I_m(x,\mu) \\ \dfrac{\partial}{\partial\tau} I_m(\tau,\mu) = c \dfrac{\partial}{\partial x} I_m(x,\mu) \end{cases} \tag{45}$$

To simplify the notation, for the remainder of this manuscript, we give for granted the x and μ dependency and write the terms for the forward and backward flux as I_m^+ and I_m^-, respectively. Thus, our problem becomes:

$$c\mu_i \frac{\partial}{\partial x} I_m^+ + I_m^+ = \frac{\omega}{2} \sum_{l=m}^{L} \beta_l P_l^m(\mu_i) \sum_{k=1}^{N} w_k P_l^m(\mu_k)[I_m^+ + (-1)^{l-m} I_m^-] + \frac{\omega}{2} e^{-\tau/\mu_0} \sum_{l=m}^{L} \beta_l P_l^m(\mu_0) P_l^m(\mu_i) \tag{46}$$

$$-c\mu_i \frac{\partial}{\partial x} I_m^- + I_m^- = \frac{\omega}{2} \sum_{l=m}^{L} \beta_l P_l^m(-\mu_i) \sum_{k=1}^{N} w_k P_l^m(-\mu_k)[(-1)^{l-m} I_m^+ + I_m^-] + \frac{\omega}{2} e^{-\tau/\mu_0} \sum_{l=m}^{L} \beta_l P_l^m(\mu_0) P_l^m(-\mu_i) \tag{47}$$

Subject to:

$$\begin{cases} I_m^+(0) = I_0^+ = 0 \\ I_m^-(\tau_0) = I_f^- = 0 \end{cases} \tag{48}$$

Our constrained expressions, for forward and backward terms, are:

$$I_m^{\pm}(x) = g^{\pm}(x) + \eta^{\pm} \tag{49}$$

Therefore, by using the boundary conditions to calculate η^+ and η^-, we obtain:

$$I_0^+ = 0 = g_0^+ + \eta^+ \qquad \longrightarrow \quad \eta^+ = -g_0^+$$
$$I_f^- = 0 = g_f^- + \eta^- \qquad \longrightarrow \quad \eta^- = -g_f^-$$

and then:

$$I_m^+(x) = g^+(x) - g_0^+$$
$$I_m^-(x) = g^-(x) - g_f^-$$

Finally, we get the CEs for the fluxes in the following form:

$$I_m^+ = (\boldsymbol{h}^T - \boldsymbol{h_0}^T)\boldsymbol{\xi}^+ \qquad ; \qquad I_m^- = (\boldsymbol{h}^T - \boldsymbol{h_f}^T)\boldsymbol{\xi}^-, \tag{50}$$

where $\boldsymbol{\xi}^+$ and $\boldsymbol{\xi}^-$ are the unknowns to be computed via LS. Plugging (50) into our DEs, we get:

$$c\mu_i \boldsymbol{h'}^T \boldsymbol{\xi}_i^+ + (\boldsymbol{h} - \boldsymbol{h_0})^T \boldsymbol{\xi}_i^+ =$$
$$= \frac{\omega}{2} \sum_{l=m}^{L} \beta_l P_l^m(\mu_i) \sum_{k=1}^{N} w_k P_l^m(\mu_k)[(\boldsymbol{h} - \boldsymbol{h_0})^T \boldsymbol{\xi}_k^+ + (-1)^{l-m} (\boldsymbol{h} - \boldsymbol{h_f})^T \boldsymbol{\xi}_k^-] + \frac{\omega}{2} e^{-\tau/\mu_0} \sum_{l=m}^{L} \beta_l P_l^m(\mu_0) P_l^m(\mu_i) \tag{51}$$

$$-c\mu_i \boldsymbol{h'}^T \boldsymbol{\xi}_i^- + (\boldsymbol{h} - \boldsymbol{h_f})^T \boldsymbol{\xi}_i^- =$$
$$= \frac{\omega}{2} \sum_{l=m}^{L} \beta_l P_l^m(-\mu_i) \sum_{k=1}^{N} w_k P_l^m(-\mu_k)[(-1)^{l-m} (\boldsymbol{h} - \boldsymbol{h_0})^T \boldsymbol{\xi}_k^+ + (\boldsymbol{h} - \boldsymbol{h_f})^T \boldsymbol{\xi}_k^-] + \frac{\omega}{2} e^{-\tau/\mu_0} \sum_{l=m}^{L} \beta_l P_l^m(\mu_0) P_l^m(-\mu_i) \tag{52}$$

Reorganizing all the terms we get:

$$(c\mu_i \boldsymbol{h'} + \boldsymbol{h} - \boldsymbol{h_0})^T \boldsymbol{\xi}_i^+ - \frac{\omega}{2} \sum_{l=m}^{L} \beta_l P_l^m(\mu_i) \sum_{k=1}^{N} w_k P_l^m(\mu_k)[(\boldsymbol{h} - \boldsymbol{h_0})^T \boldsymbol{\xi}_k^+ + (-1)^{l-m} (\boldsymbol{h} - \boldsymbol{h_f})^T \boldsymbol{\xi}_k^-] =$$
$$= \frac{\omega}{2} e^{-\tau/\mu_0} \sum_{l=m}^{L} \beta_l P_l^m(\mu_0) P_l^m(\mu_i) \tag{53}$$

$$(-c\mu_i \boldsymbol{h'} + \boldsymbol{h} - \boldsymbol{h_f})^T \boldsymbol{\xi}_i^- - \frac{\omega}{2} \sum_{l=m}^{L} \beta_l P_l^m(-\mu_i) \sum_{k=1}^{N} w_k P_l^m(-\mu_k)[(-1)^{l-m} (\boldsymbol{h} - \boldsymbol{h_0})^T \boldsymbol{\xi}_k^+ + (\boldsymbol{h} - \boldsymbol{h_f})^T \boldsymbol{\xi}_k^-] =$$
$$= \frac{\omega}{2} e^{-\tau/\mu_0} \sum_{l=m}^{L} \beta_l P_l^m(\mu_0) P_l^m(-\mu_i) \tag{54}$$

For the sake of simplicity, we write the inhomogeneous term as:

$$\boldsymbol{b_i^+} = \frac{\omega}{2} e^{-\tau/\mu_0} \sum_{l=m}^{L} \beta_l P_l^m(\mu_0) P_l^m(\mu_i) \qquad\qquad \boldsymbol{b_i^-} = \frac{\omega}{2} e^{-\tau/\mu_0} \sum_{l=m}^{L} \beta_l P_l^m(\mu_0) P_l^m(-\mu_i)$$

So, the two problems become:

$$(c\mu_i \boldsymbol{h'} + \boldsymbol{h} - \boldsymbol{h_0})^T \boldsymbol{\xi}_i^+ - \frac{\omega}{2} \sum_{l=m}^{L} \beta_l P_l^m(\mu_i) \sum_{k=1}^{N} w_k P_l^m(\mu_k)[(\boldsymbol{h} - \boldsymbol{h_0})^T \boldsymbol{\xi}_k^+ + (-1)^{l-m} (\boldsymbol{h} - \boldsymbol{h_f})^T \boldsymbol{\xi}_k^-] = \boldsymbol{b_i^+} \quad (55)$$

$$(-c\mu_i \boldsymbol{h'} + \boldsymbol{h} - \boldsymbol{h_f})^T \boldsymbol{\xi}_i^- - \frac{\omega}{2} \sum_{l=m}^{L} \beta_l P_l^m(-\mu_i) \sum_{k=1}^{N} w_k P_l^m(-\mu_k)[(-1)^{l-m} (\boldsymbol{h} - \boldsymbol{h_0})^T \boldsymbol{\xi}_k^+ + (\boldsymbol{h} - \boldsymbol{h_f})^T \boldsymbol{\xi}_k^-] = \boldsymbol{b_i^-} \quad (56)$$

Expanding the summations, we get the following matrix form:

$$\begin{bmatrix} \bigstar_i + \blacklozenge_i^k & \clubsuit_i^k \\ \spadesuit_i^k & \blacktriangledown_i + \heartsuit_i^k \end{bmatrix} \begin{bmatrix} \boldsymbol{\xi_i^+} \\ \boldsymbol{\xi_i^-} \end{bmatrix} = \begin{bmatrix} \boldsymbol{b_i^+} \\ \boldsymbol{b_i^-} \end{bmatrix} \quad (57)$$

where:

$$\blacktriangledown_i = (-c\mu_i \boldsymbol{h'} + \boldsymbol{h} - \boldsymbol{h_f})^T$$

$$\bigstar_i = (c\mu_i \boldsymbol{h'} + \boldsymbol{h} - \boldsymbol{h_0})^T$$

$$\clubsuit_i^k = -\frac{\omega}{2} w_k (\boldsymbol{h} - \boldsymbol{h_f})^T \sum_{l=m}^{L} \beta_l P_l^m(\mu_i) P_l(\mu_k) (-1)^{l-m}$$

$$\spadesuit_i^k = -\frac{\omega}{2} w_k (\boldsymbol{h} - \boldsymbol{h_0})^T \sum_{l=m}^{L} \beta_l P_l^m(-\mu_i) P_l(-\mu_k) (-1)^{l-m}$$

$$\blacklozenge_i^k = -\frac{\omega}{2} w_k (\boldsymbol{h} - \boldsymbol{h_0})^T \sum_{l=m}^{L} \beta_l P_l^m(\mu_i) P_l(\mu_k)$$

$$\heartsuit_i^k = -\frac{\omega}{2} w_k (\boldsymbol{h} - \boldsymbol{h_f})^T \sum_{l=m}^{L} \beta_l P_l^m(-\mu_i) P_l(-\mu_k)$$

Thus, the problem reduce to the following linear system of algebraic equations:

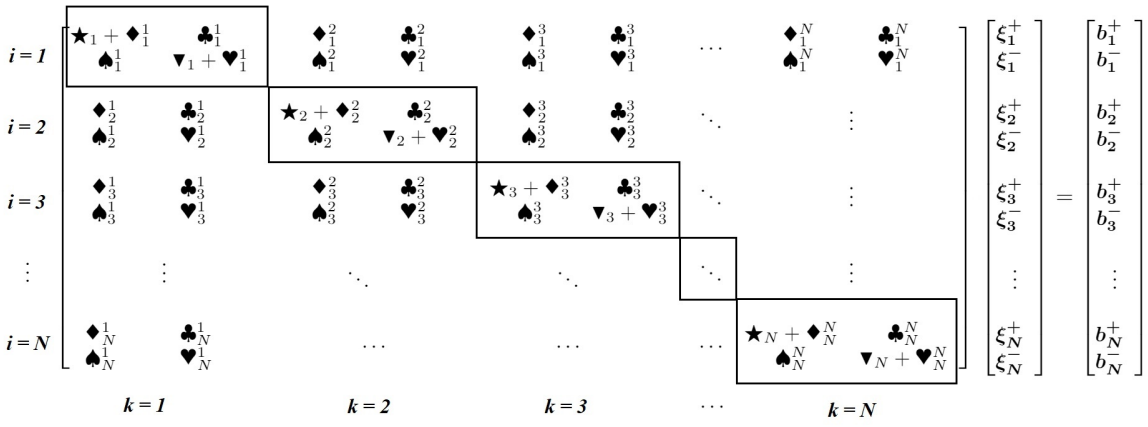

which is a problem of the type:

$$\boldsymbol{A\xi} = \boldsymbol{B} \quad (58)$$

whose the dimensions are:

$$\boldsymbol{\xi}^{\pm}_{\boldsymbol{i}\,[m_{op} \times 1]}$$

$$\boldsymbol{\xi}_{[2m_{op}\,N \times 1]}$$

$$\boldsymbol{b}^{\pm}_{\boldsymbol{i}\,[M\times 1]}$$

$$\boldsymbol{B}_{[2MN\times 1]}$$

$\bigstar_{\boldsymbol{i}\,[M\times m_{op}]}$ (same dimension for the other terms of the matrix $\boldsymbol{A}$)

$$\boldsymbol{A}_{[(2MN)\times(2m_{op}\,N)]}$$

where M is the number of discretization points of τ, and m_{op} is the number of basis functions used.
That is, the original Linear BVP has been reformulated as an *unconstrained* optimization problem. In this case, $\boldsymbol{\xi}$ is calculated with only one direct pass via LS methods, as the original problem is linear [21]. That is:

$$\boldsymbol{\xi} = \left(\boldsymbol{A}^T\boldsymbol{A}\right)^{-1}\boldsymbol{A}^T\boldsymbol{B} \tag{59}$$

As can be seen from 59 the unknowns are computed using a classic LS method. However, the authors have tried all the LS methods suggested in Appendix A of reference [22], find the classic LS method the most convenient in terms of accuracy and computational time.
Once $\boldsymbol{\xi}$ are computed, the final solutions are built according to (50).
After finding the solutions for all m^{th} Fourier components (with $m = 0, 1, ..., L$), we can compute the diffuse terms expressed as:

$$I(\tau,\mu,\phi) = \frac{1}{2}\sum_{m=0}^{L}(2-\delta_{0,m})I_m(\tau,\mu)\cos[m(\phi-\phi_0)] \tag{60}$$

$$I(\tau,-\mu,\phi) = \frac{1}{2}\sum_{m=0}^{L}(2-\delta_{0,m})I_m(\tau,-\mu)\cos[m(\phi-\phi_0)] \tag{61}$$

For the convenience of the reader, the all process described in this section is summarized in the schematic of Fig. 3.

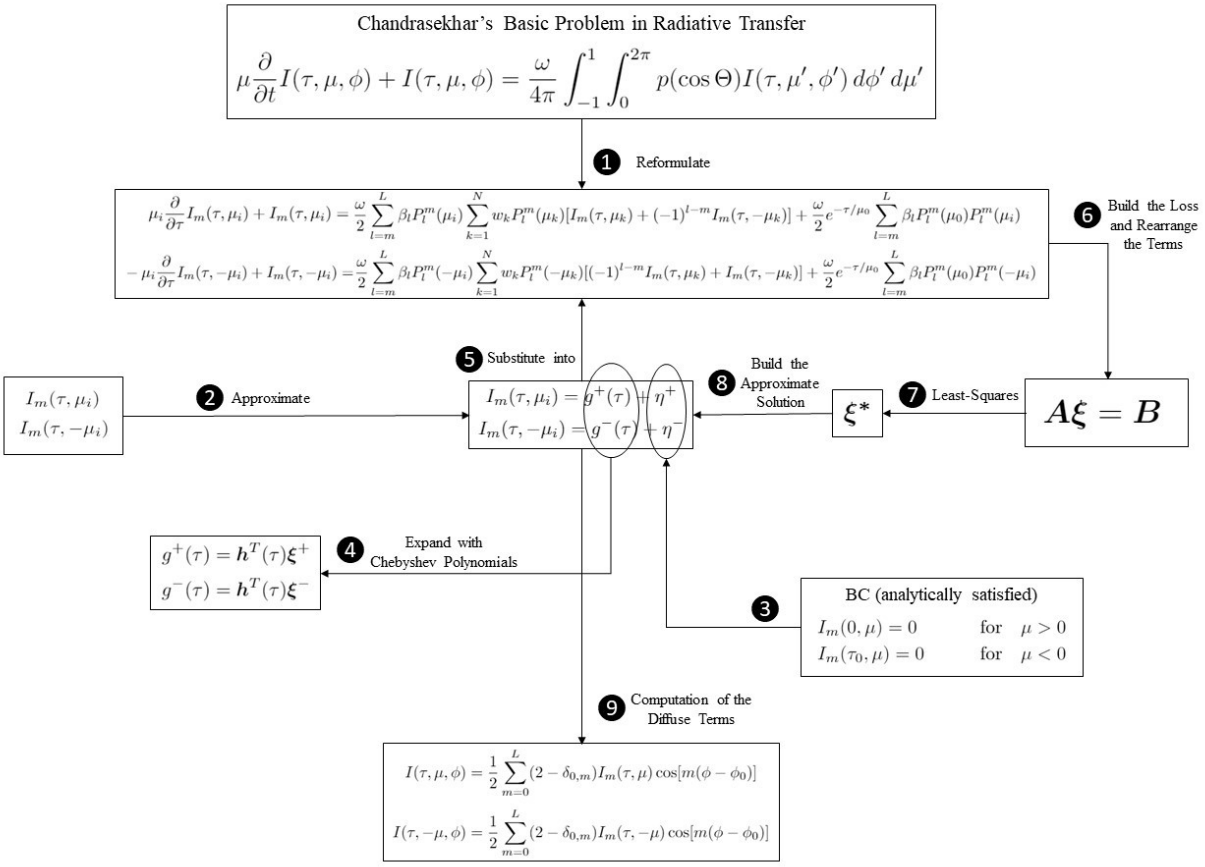

Figure 3: Schematic of the Theory of Functional Connections algorithm to solve Chandrasekhar's Basic Problem in Radiative Transfer.

5. Post-Processing

Via the discretization of the cosine of the polar angle μ , the solutions obtained are for specific angles μ that are the Gauss–Legendre quadrature nodes. However, in many applications, it is necessary to compute the solutions for any arbitrary angles, that can be different than the Gauss–Legendre quadrature nodes. To compute the solutions at any arbitrary query points μ a post–processing is needed. The post–processing is also performed via TFC. Introducing some changes to the equations (55) and (56), we get:

$$(c\gamma_j \boldsymbol{h'} + \boldsymbol{h} - \boldsymbol{h_0})^T \boldsymbol{\zeta}_j^+ = \frac{\omega}{2} \sum_{l=m}^{L} \beta_l P_l^m(\gamma_j) \sum_{k=1}^{N} w_k P_l^m(\mu_k)[(\boldsymbol{h} - \boldsymbol{h_0})^T \boldsymbol{\xi}_k^+ + (-1)^{l-m} (\boldsymbol{h} - \boldsymbol{h_f})^T \boldsymbol{\xi}_k^-] + \boldsymbol{b_i^+} \quad (62)$$

$$(-c\gamma_j \boldsymbol{h'} + \boldsymbol{h} - \boldsymbol{h_f})^T \boldsymbol{\zeta}_j^- = \frac{\omega}{2} \sum_{l=m}^{L} \beta_l P_l^m(-\gamma_j) \sum_{k=1}^{N} w_k P_l^m(-\mu_k)[(-1)^{l-m} (\boldsymbol{h} - \boldsymbol{h_0})^T \boldsymbol{\xi}_k^+ + (\boldsymbol{h} - \boldsymbol{h_f})^T \boldsymbol{\xi}_k^-] + \boldsymbol{b_i^-} \quad (63)$$

where γ_j are the query angles, and $\boldsymbol{\zeta_j^{\pm}}$ are the vectors of the new unknowns corresponding to the angle γ_j, and the right–hand sides of the equations are known. Hence, we obtain the following linear system:

$$\left(c\gamma_j \boldsymbol{h'} + \boldsymbol{h} - \boldsymbol{h_0}\right)^T \boldsymbol{\zeta}_j^+ = \frac{\omega}{2} \sum_{l=m}^{L} \beta_l P_l^m(\gamma_j) \sum_{k=1}^{N} w_k P_l^m(\mu_k) \left[(\boldsymbol{h} - \boldsymbol{h_0})^T \boldsymbol{\xi}_k^+ + (-1)^{l-m} (\boldsymbol{h} - \boldsymbol{h_f})^T \boldsymbol{\xi}_k^-\right] + \boldsymbol{b_i^+} \quad (64)$$

$$\left(-c\gamma_j \boldsymbol{h'} + \boldsymbol{h} - \boldsymbol{h_f}\right)^T \boldsymbol{\zeta}_j^- = \frac{\omega}{2} \sum_{l=m}^{L} \beta_l P_l^m(\gamma_j) \sum_{k=1}^{N} w_k P_l^m(-\mu_k) \left[(-1)^{l-m} (\boldsymbol{h} - \boldsymbol{h_0})^T \boldsymbol{\xi}_k^+ + (\boldsymbol{h} - \boldsymbol{h_f})^T \boldsymbol{\xi}_k^-\right] + \boldsymbol{b_i^-} \quad (65)$$

This is solved for $\boldsymbol{\zeta_j^{\pm}}$ via LS. Once $\boldsymbol{\zeta_j^{\pm}}$ are computed, the final solutions are again built according to (50). After finding the solutions for all m^{th} Fourier components (with $m = 0, 1, ..., L$) we can compute the diffuse terms as follows:

$$I^+(\tau, \gamma, \phi) = \frac{1}{2} \sum_{m=0}^{L} (2 - \delta_{0,m}) I_m^+(\tau, \gamma) \cos[m(\phi - \phi_0)] \quad (66)$$

$$I^-(\tau, -\gamma, \phi) = \frac{1}{2} \sum_{m=0}^{L} (2 - \delta_{0,m}) I_m^-(\tau, -\gamma) \cos[m(\phi - \phi_0)] \quad (67)$$

6. Results and Discussions

The algorithm described above has been implemented in both Matlab and Python platforms. To validate the accuracy of our framework, we compared our results with some of typical benchmarks for the Radiative Transfer problems, such as Mie Scattering and Haze L Problem. We ran all our simulations with an Intel Core i7 - 9700 CPU PC with 64 GB of RAM. The results reported below are obtained via Matlab, although the ones computed with Python achieved the same order of accuracy.

The first benchmark of interest is the Radiative Transfer problem with scattering modeled via the Mie Scattering theory for spherical particles. This problem is defined by a $L = 8$ phase function. The results obtained using the TFC approach are compared with the benchmarks reported by Garcia and Siewert (1986) [31]. The latter employed a discretization of $N = 20 - 50$ μ directions. Our results are reported in tables 3-11 , where thee following the following parameters have been employed: $N = 15$, $M = 100$, $m_{op} = 40$, $\tau_0 = 1$, $S_0 = 1$, $\mu_0 = 0.5$, $\omega = 0.95$. The TFC algorithm achieved the reported results with a computational time of 0.026 seconds. Importantly, the TFC method achieved exactly the same results as reported by Garcia and Siewert [31].

Table 3: Mie Scattering – The Fourier Component $I_*(\tau, \mu)$ for $m = 0$, with a computational time of approximately 0.026 seconds.

$\boldsymbol{\mu}$	$\boldsymbol{\tau = 0}$	$\boldsymbol{\tau = 0.05\tau_0}$	$\boldsymbol{\tau = 0.1\tau_0}$	$\boldsymbol{\tau = 0.2\tau_0}$	$\boldsymbol{\tau = 0.5\tau_0}$	$\boldsymbol{\tau = 0.75\tau_0}$	$\boldsymbol{\tau = \tau_0}$
-1.0	4.76807e-2	4.41912e-2	4.06467e-2	3.37099e-2	1.58572e-2	5.45297e-3	0
-0.9	6.45644e-2	6.03742e-2	5.60139e-2	4.72899e-2	2.38121e-2	9.01083e-3	0
-0.8	8.45877e-2	7.96763e-2	7.44425e-2	6.37540e-2	3.38287e-2	1.36919e-2	0
-0.7	1.08350e-1	1.02719e-1	9.65678e-2	8.37488e-2	4.64918e-2	1.98845e-2	0
-0.6	1.36504e-1	1.30204e-1	1.23128e-1	1.08063e-1	6.26048e-2	2.81721e-2	0
-0.5	1.69677e-1	1.62852e-1	1.54919e-1	1.37618e-1	8.32921e-2	3.94792e-2	0
-0.4	2.08230e-1	2.01201e-1	1.92626e-1	1.73358e-1	1.10124e-1	5.53631e-2	0
-0.3	2.51677e-1	2.45065e-1	2.36310e-1	2.15806e-1	1.45144e-1	7.86298e-2	0
-0.2	2.97523e-1	2.92401e-1	2.84241e-1	2.63800e-1	1.90035e-1	1.14557e-1	0
-0.1	3.40126e-1	3.38476e-1	3.31984e-1	3.12888e-1	2.41217e-1	1.70697e-1	0
-0.0	3.59379e-1	3.74485e-1	3.73800e-1	3.59347e-1	2.88258e-1	2.25623e-1	0
0.0	0	3.74485e-1	3.73800e-1	3.59347e-1	2.88258e-1	2.25623e-1	1.51520e-1
0.1	0	1.55620e-1	2.51427e-1	3.38864e-1	3.30703e-1	2.69855e-1	2.03073e-1
0.2	0	9.24370e-2	1.65080e-1	2.61887e-1	3.35517e-1	3.01553e-1	2.44242e-1
0.3	0	6.70726e-2	1.24144e-1	2.10383e-1	3.14805e-1	3.09713e-1	2.70302e-1
0.4	0	5.30170e-2	9.98939e-2	1.75304e-1	2.88183e-1	3.02939e-1	2.81066e-1
0.5	0	4.37182e-2	8.32383e-2	1.49251e-1	2.61304e-1	2.88464e-1	2.80822e-1
0.6	0	3.67864e-2	7.05194e-2	1.28323e-1	2.35259e-1	2.69793e-1	2.73029e-1
0.7	0	3.11411e-2	5.99908e-2	1.10387e-1	2.09939e-1	2.48476e-1	2.59822e-1
0.8	0	2.62225e-2	5.07166e-2	9.42001e-2	1.84982e-1	2.25179e-1	2.42453e-1
0.9	0	2.17133e-2	4.21538e-2	7.90039e-2	1.60034e-1	2.00187e-1	2.21667e-1
1.0	0	1.74231e-2	3.39716e-2	6.43193e-2	1.34819e-1	1.73627e-1	1.97932e-1

Table 4: Mie Scattering – The Fourier Component $I_*(\tau, \mu)$ for $m = 1$, with a computational time of approximately 0.026 seconds.

$\boldsymbol{\mu}$	$\boldsymbol{\tau = 0}$	$\boldsymbol{\tau = 0.05\tau_0}$	$\boldsymbol{\tau = 0.1\tau_0}$	$\boldsymbol{\tau = 0.2\tau_0}$	$\boldsymbol{\tau = 0.5\tau_0}$	$\boldsymbol{\tau = 0.75\tau_0}$	$\boldsymbol{\tau = \tau_0}$
-1.0	0	0	0	0	0	0	0
-0.9	3.60181e-2	3.36746e-2	3.12064e-2	2.62787e-2	1.32903e-2	5.19802e-3	0
-0.8	6.16596e-2	5.78589e-2	5.38160e-2	4.56764e-2	2.38338e-2	9.72915e-3	0
-0.7	9.10359e-2	8.57207e-2	8.00113e-2	6.84223e-2	3.67820e-2	1.56203e-2	0
-0.6	1.26254e-1	1.19295e-1	1.11742e-1	9.62823e-2	5.33398e-2	2.35586e-2	0
-0.5	1.68911e-1	1.60192e-1	1.50609e-1	1.30818e-1	7.48561e-2	3.44878e-2	0
-0.4	2.20425e-1	2.09925e-1	1.98188e-1	1.73691e-1	1.03142e-1	4.99460e-2	0
-0.3	2.81715e-1	2.69635e-1	2.55778e-1	2.26467e-1	1.40633e-1	7.26822e-2	0
-0.2	3.52226e-1	3.39192e-1	3.23503e-1	2.89666e-1	1.89868e-1	1.07900e-1	0
-0.1	4.28566e-1	4.16266e-1	3.99406e-1	3.61374e-1	2.49443e-1	1.63513e-1	0
-0.0	4.90592e-1	4.93468e-1	4.79629e-1	4.40175e-1	3.12405e-1	2.22786e-1	0
0.0	0	4.93468e-1	4.79629e-1	4.40175e-1	3.12405e-1	2.22786e-1	1.40086e-1
0.1	0	2.12101e-1	3.36358e-1	4.36674e-1	3.78485e-1	2.79507e-1	1.92369e-1
0.2	0	1.27652e-1	2.24094e-1	3.44034e-1	3.98038e-1	3.26312e-1	2.41187e-1
0.3	0	9.31423e-2	1.69547e-1	2.78455e-1	3.79153e-1	3.42883e-1	2.74467e-1
0.4	0	7.34351e-2	1.36109e-1	2.31599e-1	3.47468e-1	3.37079e-1	2.87903e-1
0.5	0	5.97940e-2	1.11999e-1	1.94715e-1	3.11216e-1	3.17429e-1	2.84863e-1
0.6	0	4.89801e-2	9.23641e-2	1.62887e-1	2.72157e-1	2.88095e-1	2.68557e-1
0.7	0	3.94407e-2	7.47181e-2	1.33107e-1	2.29842e-1	2.50372e-1	2.40503e-1
0.8	0	3.01812e-2	5.73658e-2	1.02969e-1	1.82413e-1	2.03320e-1	2.00130e-1
0.9	0	2.00568e-2	3.82174e-2	6.90058e-2	1.24817e-1	1.41801e-1	1.42461e-1
1.0	0	0	0	0	0	0	0

Table 5: Mie Scattering – The Fourier Component $I_*(\tau, \mu)$ for $m = 2$, with a computational time of approximately 0.026 seconds.

$\boldsymbol{\mu}$	$\boldsymbol{\tau = 0}$	$\boldsymbol{\tau = 0.05\tau_0}$	$\boldsymbol{\tau = 0.1\tau_0}$	$\boldsymbol{\tau = 0.2\tau_0}$	$\boldsymbol{\tau = 0.5\tau_0}$	$\boldsymbol{\tau = 0.75\tau_0}$	$\boldsymbol{\tau = \tau_0}$
-1.0	0	0	0	0	0	0	0
-0.9	6.13369e-3	5.63258e-3	5.14146e-3	4.22728e-3	2.08109e-3	8.51138e-4	0
-0.8	1.40473e-2	1.29199e-2	1.18125e-2	9.74639e-3	4.86758e-3	2.02908e-3	0
-0.7	2.42374e-2	2.23272e-2	2.04470e-2	1.69330e-2	8.59010e-3	3.65704e-3	0
-0.6	3.72977e-2	3.44146e-2	3.15724e-2	2.62520e-2	1.35554e-2	5.91266e-3	0
-0.5	5.39364e-2	4.98590e-2	4.58321e-2	3.82838e-2	2.01851e-2	9.06805e-3	0
-0.4	7.49853e-2	6.94667e-2	6.40030e-2	5.37486e-2	2.90737e-2	1.35709e-2	0
-0.3	1.01366e-1	9.41479e-2	8.69734e-2	7.34927e-2	4.10537e-2	2.02184e-2	0
-0.2	1.33969e-1	1.24806e-1	1.15624e-1	9.83434e-2	5.71259e-2	3.05232e-2	0
-0.1	1.73539e-1	1.62321e-1	1.50803e-1	1.28934e-1	7.75407e-2	4.68764e-2	0
-0.0	2.17610e-1	2.07223e-1	1.93748e-1	1.66780e-1	1.01645e-1	6.54823e-2	0
0.0	0	2.07223e-1	1.93748e-1	1.66780e-1	1.01645e-1	6.54823e-2	3.94802e-2
0.1	0	9.13850e-2	1.41198e-1	1.74338e-1	1.30506e-1	8.62088e-2	5.45248e-2
0.2	0	5.47834e-2	9.40008e-2	1.38386e-1	1.41997e-1	1.05409e-1	7.12370e-2
0.3	0	3.94265e-2	7.02551e-2	1.11034e-1	1.35966e-1	1.12775e-1	8.32078e-2
0.4	0	3.03255e-2	5.50820e-2	9.03843e-2	1.22905e-1	1.10240e-1	8.74206e-2
0.5	0	2.37574e-2	4.36468e-2	7.32857e-2	1.06676e-1	1.01104e-1	8.46547e-2
0.6	0	1.83638e-2	3.39907e-2	5.79582e-2	8.84652e-2	8.72842e-2	7.61525e-2
0.7	0	1.35348e-2	2.51835e-2	4.34139e-2	6.86137e-2	6.97897e-2	6.28579e-2
0.8	0	8.96183e-3	1.67383e-2	2.90913e-2	4.72161e-2	4.91804e-2	4.54269e-2
0.9	0	4.47932e-3	8.39018e-3	1.46739e-2	2.43199e-2	2.58191e-2	2.43409e-2
1.0	0	0	0	0	0	0	0

Table 6: Mie Scattering – The Fourier Component $I_*(\tau, \mu)$ for $m = 3$, with a computational time of approximately 0.026 seconds.

$\boldsymbol{\mu}$	$\boldsymbol{\tau = 0}$	$\boldsymbol{\tau = 0.05\tau_0}$	$\boldsymbol{\tau = 0.1\tau_0}$	$\boldsymbol{\tau = 0.2\tau_0}$	$\boldsymbol{\tau = 0.5\tau_0}$	$\boldsymbol{\tau = 0.75\tau_0}$	$\boldsymbol{\tau = \tau_0}$
-1.0	0	0	0	0	0	0	0
-0.9	4.71882e-4	4.27922e-4	3.86504e-4	3.12323e-4	1.49303e-4	6.12974e-5	0
-0.8	1.63700e-3	1.48492e-3	1.34202e-3	1.e-08650e-3	5.24875e-4	2.18940e-4	0
-0.7	3.62794e-3	3.29256e-3	2.97807e-3	2.41643e-3	1.18117e-3	5.01304e-4	0
-0.6	6.65125e-3	6.04087e-3	5.46943e-3	4.44992e-3	2.20550e-3	9.55263e-4	0
-0.5	1.09558e-2	9.96046e-3	9.02968e-3	7.37068e-3	3.71563e-3	1.65092e-3	0
-0.4	1.68361e-2	1.53260e-2	1.39154e-2	1.14039e-2	5.87321e-3	2.70031e-3	0
-0.3	2.46361e-2	2.24603e-2	2.04291e-2	1.68191e-2	8.90196e-3	4.29905e-3	0
-0.2	3.47536e-2	3.17326e-2	2.89122e-2	2.39119e-2	1.30799e-2	6.81521e-3	0
-0.1	4.77051e-2	4.36203e-2	3.97892e-2	3.29968e-2	1.85468e-2	1.08405e-2	0
-0.0	6.40589e-2	5.89247e-2	5.38601e-2	4.47620e-2	2.52999e-2	1.55900e-2	0
0.0	0	5.89247e-2	5.38601e-2	4.47620e-2	2.52999e-2	1.55900e-2	9.40491e-3
0.1	0	2.65947e-2	4.04696e-2	4.85984e-2	3.37870e-2	2.12142e-2	1.30156e-2
0.2	0	1.59125e-2	2.69468e-2	3.87779e-2	3.75052e-2	2.66263e-2	1.73623e-2
0.3	0	1.12859e-2	1.98696e-2	3.07668e-2	3.58014e-2	2.85953e-2	2.04272e-2
0.4	0	8.43804e-3	1.51551e-2	2.44012e-2	3.16829e-2	2.74886e-2	2.11807e-2
0.5	0	6.31959e-3	1.14883e-2	1.89493e-2	2.64242e-2	2.42961e-2	1.98181e-2
0.6	0	4.56717e-3	8.36998e-3	1.40335e-2	2.05701e-2	1.97297e-2	1.67997e-2
0.7	0	3.04358e-3	5.61002e-3	9.51751e-3	1.44725e-2	1.43314e-2	1.26141e-2
0.8	0	1.71669e-3	3.17792e-3	5.43950e-3	8.50729e-3	8.63650e-3	7.80304e-3
0.9	0	6.32858e-4	1.17545e-3	2.02593e-3	3.23965e-3	3.35492e-3	3.09582e-3
1.0	0	0	0	0	0	0	0

Table 7: Mie Scattering – The Fourier Component $I_*(\tau, \mu)$ for $m = 4$, with a computational time of approximately 0.026 seconds.

$\boldsymbol{\mu}$	$\boldsymbol{\tau = 0}$	$\boldsymbol{\tau = 0.05\tau_0}$	$\boldsymbol{\tau = 0.1\tau_0}$	$\boldsymbol{\tau = 0.2\tau_0}$	$\boldsymbol{\tau = 0.5\tau_0}$	$\boldsymbol{\tau = 0.75\tau_0}$	$\boldsymbol{\tau = \tau_0}$
-1.0	0	0	0	0	0	0	0
-0.9	6.69258e-5	6.02239e-5	5.40838e-5	4.33436e-5	2.05304e-5	0.851494e-6	0
-0.8	3.02494e-4	2.72377e-4	2.44794e-4	1.96548e-4	9.39014e-5	3.93973e-5	0
-0.7	7.61720e-4	6.86418e-4	6.17472e-4	4.96877e-4	2.39851e-4	1.02062e-4	0
-0.6	1.50358e-3	1.35622e-3	1.22134e-3	9.85431e-4	4.81766e-4	2.08696e-4	0
-0.5	2.59147e-3	2.34013e-3	2.11014e-3	1.70803e-3	8.48455e-4	3.76292e-4	0
-0.4	4.09363e-3	3.70143e-3	3.34275e-3	2.71612e-3	1.37699e-3	6.30869e-4	0
-0.3	6.08324e-3	5.50815e-3	4.98269e-3	4.06626e-3	2.11599e-3	1.01667e-3	0
-0.2	8.63901e-3	7.83189e-3	7.09526e-3	5.81430e-3	3.12207e-3	1.61559e-3	0
-0.1	1.18659e-2	1.07645e-2	9.75898e-3	8.01357e-3	4.41270e-3	2.55497e-3	0
-0.0	1.59510e-2	1.44948e-2	1.31484e-2	1.08036e-2	5.96834e-3	3.63154e-3	0
0.0	0	1.44948e-2	1.31484e-2	1.08036e-2	5.96834e-3	3.63154e-3	2.19670e-3
0.1	0	6.42599e-3	9.72886e-3	1.15783e-2	7.86933e-3	4.86919e-3	2.96365e-3
0.2	0	3.72830e-3	6.28643e-3	8.98115e-3	8.53292e-3	5.98094e-3	3.86184e-3
0.3	0	2.53962e-3	4.45371e-3	6.85213e-3	7.85349e-3	6.20648e-3	4.39482e-3
0.4	0	1.80267e-3	3.22602e-3	5.16374e-3	6.61455e-3	5.68628e-3	4.34786e-3
0.5	0	1.26267e-3	2.28772e-3	3.75288e-3	5.16865e-3	4.71326e-3	3.81819e-3
0.6	0	8.35644e-4	1.52664e-3	2.54654e-3	3.68968e-3	3.51216e-3	2.97182e-3
0.7	0	4.93531e-4	9.07021e-4	1.53136e-3	2.30332e-3	2.26473e-3	1.98170e-3
0.8	0	2.32528e-4	4.29264e-4	7.31400e-4	1.13210e-3	1.14161e-3	1.02575e-3
0.9	0	6.20029e-5	1.14862e-4	1.97113e-4	3.12097e-4	3.21141e-4	2.94782e-4
1.0	0	0	0	0	0	0	0

Table 8: Mie Scattering – The Fourier Component $I_*(\tau, \mu)$ for $m = 5$, with a computational time of approximately 0.026 seconds.

$\boldsymbol{\mu}$	$\boldsymbol{\tau = 0}$	$\boldsymbol{\tau = 0.05\tau_0}$	$\boldsymbol{\tau = 0.1\tau_0}$	$\boldsymbol{\tau = 0.2\tau_0}$	$\boldsymbol{\tau = 0.5\tau_0}$	$\boldsymbol{\tau = 0.75\tau_0}$	$\boldsymbol{\tau = \tau_0}$
-1.0	0	0	0	0	0	0	0
-0.9	6.28063e-6	5.64038e-6	5.05780e-6	4.04469e-6	1.91071e-6	7.93886e-7	0
-0.8	3.73124e-5	3.35331e-5	3.00940e-5	2.41116e-5	1.14857e-5	4.82442e-6	0
-0.7	1.07458e-4	9.66557e-5	8.68253e-5	6.97210e-5	3.35504e-5	1.42849e-5	0
-0.6	2.29470e-4	2.06608e-4	1.85802e-4	1.49599e-4	7.28951e-5	3.15824e-5	0
-0.5	4.15167e-4	3.74235e-4	3.36993e-4	2.72200e-4	1.34741e-4	5.97452e-5	0
-0.4	6.75372e-4	6.09580e-4	5.49751e-4	4.45739e-4	2.25137e-4	1.03090e-4	0
-0.3	1.01957e-3	9.21504e-4	8.32420e-4	6.77822e-4	3.51320e-4	1.68651e-4	0
-0.2	1.45558e-3	1.31706e-3	1.19142e-3	9.74059e-4	5.20758e-4	2.69137e-4	0
-0.1	1.99273e-3	1.80388e-3	1.63272e-3	1.33734e-3	7.32823e-4	4.23514e-4	0
-0.0	2.65403e-3	2.40328e-3	2.17551e-3	1.78221e-3	9.79104e-4	5.94123e-4	0
0.0	0	2.40328e-3	2.17551e-3	1.78221e-3	9.79104e-4	5.94123e-4	3.60119e-4
0.1	0	1.04360e-3	1.57774e-3	1.87309e-3	1.26582e-3	7.80603e-4	4.74525e-4
0.2	0	5.87087e-4	9.88700e-4	1.40973e-3	1.33332e-3	9.31756e-4	6.00443e-4
0.3	0	3.83898e-4	6.72490e-4	1.03283e-3	1.17920e-3	9.29569e-4	6.57017e-4
0.4	0	2.58469e-4	4.62075e-4	7.38429e-4	9.42637e-4	8.08592e-4	6.17257e-4
0.5	0	1.69091e-4	3.06064e-4	5.01326e-4	6.88265e-4	6.26405e-4	5.06701e-4
0.6	0	1.02291e-4	1.86706e-4	3.10999e-4	4.49276e-4	4.26898e-4	3.60733e-4
0.7	0	5.34205e-5	9.80933e-5	1.65394e-4	2.48078e-4	2.43517e-4	2.12817e-4
0.8	0	2.09675e-5	3.86763e-5	6.58150e-5	1.01604e-4	1.02297e-4	9.18069e-5
0.9	0	4.03113e-6	7.46208e-6	1.27901e-5	2.02003e-5	2.07549e-5	1.90300e-5
1.0	0	0	0	0	0	0	0

Table 9: Mie Scattering – The Fourier Component $I_*(\tau, \mu)$ for $m = 6$, with a computational time of approximately 0.026 seconds.

$\boldsymbol{\mu}$	$\boldsymbol{\tau = 0}$	$\boldsymbol{\tau = 0.05\tau_0}$	$\boldsymbol{\tau = 0.1\tau_0}$	$\boldsymbol{\tau = 0.2\tau_0}$	$\boldsymbol{\tau = 0.5\tau_0}$	$\boldsymbol{\tau = 0.75\tau_0}$	$\boldsymbol{\tau = \tau_0}$
-1.0	0	0	0	0	0	0	0
-0.9	3.64612e-7	3.27338e-7	2.93459e-7	2.34597e-7	1.10774e-7	4.60360e-8	0
-0.8	2.90480e-6	2.60976e-6	2.34156e-6	1.87544e-6	8.92958e-7	3.75132e-7	0
-0.7	9.72738e-6	8.74687e-6	7.85546e-6	6.30582e-6	3.03290e-6	1.29146e-6	0
-0.6	2.27862e-5	2.05098e-5	1.84403e-5	1.48421e-6	7.22835e-6	3.13189e-6	0
-0.5	4.37887e-5	3.94595e-5	3.55246e-5	2.86845e-5	1.41912e-5	6.29250e-6	0
-0.4	7.40943e-5	6.68560e-5	6.02802e-5	4.88581e-5	2.46633e-5	1.12928e-5	0
-0.3	1.14597e-4	1.03542e-4	9.35097e-5	7.61152e-5	3.94263e-5	1.89249e-5	0
-0.2	1.65614e-4	1.49803e-4	1.35478e-4	1.10719e-4	5.91524e-5	3.05665e-5	0
-0.1	2.27191e-4	2.05580e-4	1.86022e-4	1.52303e-4	8.33921e-5	4.81822e-5	0
-0.0	3.00490e-4	2.71920e-4	2.46056e-4	2.01467e-4	1.10580e-4	6.70733e-5	0
0.0	0	2.71920e-4	2.46056e-4	2.01467e-4	1.10580e-4	6.70733e-5	4.06782e-5
0.1	0	1.16112e-4	1.75494e-4	2.08255e-4	1.40600e-4	8.66594e-5	5.26746e-5
0.2	0	6.35970e-5	1.07078e-4	1.52621e-4	1.44236e-4	1.00747e-4	6.49064e-5
0.3	0	4.00550e-5	7.01511e-5	1.07705e-4	1.22887e-4	9.68330e-5	6.84233e-5
0.4	0	2.56452e-5	4.58379e-5	7.32305e-5	9.34258e-5	8.01121e-5	6.11407e-5
0.5	0	1.56977e-5	2.84085e-5	4.65197e-5	6.38310e-5	5.80755e-5	4.69672e-5
0.6	0	8.68979e-6	1.58582e-5	2.64083e-5	3.81303e-5	3.62204e-5	3.06005e-5
0.7	0	4.01435e-6	7.37013e-6	1.24236e-5	1.86253e-5	1.82779e-5	1.59706e-5
0.8	0	1.31217e-6	2.42003e-6	4.11715e-6	6.35302e-6	6.39473e-6	5.73797e-6
0.9	0	1.81710e-7	3.36316e-7	5.76320e-7	9.09821e-7	9.34571e-7	8.56760e-7
1.0	0	0	0	0	0	0	0

Table 10: Mie Scattering – The Fourier Component $I_*(\tau, \mu)$ for $m = 7$, with a computational time of approximately 0.026 seconds.

$\boldsymbol{\mu}$	$\boldsymbol{\tau = 0}$	$\boldsymbol{\tau = 0.05\tau_0}$	$\boldsymbol{\tau = 0.1\tau_0}$	$\boldsymbol{\tau = 0.2\tau_0}$	$\boldsymbol{\tau = 0.5\tau_0}$	$\boldsymbol{\tau = 0.75\tau_0}$	$\boldsymbol{\tau = \tau_0}$
-1.0	0	0	0	0	0	0	0
-0.9	1.27031e-8	1.14041e-8	1.02235e-8	8.17255e-9	3.85880e-9	1.60370e-9	0
-0.8	1.42973e-7	1.28447e-7	1.15244e-7	9.22992e-8	4.39445e-8	1.84614e-8	0
-0.7	5.79668e-7	5.21220e-7	4.68089e-7	3.75735e-7	1.80707e-7	7.69491e-8	0
-0.6	1.53649e-6	1.38294e-6	1.24336e-6	1.00071e-6	4.87335e-7	2.11154e-7	0
-0.5	3.21082e-6	2.89328e-6	2.60469e-6	2.10309e-6	1.04041e-6	4.61327e-7	0
-0.4	5.75018e-6	5.18825e-6	4.67782e-6	3.79130e-6	1.91370e-6	8.76244e-7	0
-0.3	9.22443e-6	8.33427e-6	7.52656e-6	6.12622e-6	3.17306e-6	1.52308e-6	0
-0.2	1.36060e-5	1.23065e-5	1.11294e-5	9.09502e-6	4.85872e-6	2.51067e-6	0
-0.1	1.87914e-5	1.70031e-5	1.53850e-5	1.25956e-5	6.89601e-6	3.98428e-6	0
-0.0	2.47201e-5	2.23679e-5	2.02394e-5	1.65707e-5	9.09428e-6	5.51598e-6	0
0.0	0	2.23679e-5	2.02394e-5	1.65707e-5	9.09428e-6	5.51598e-6	3.34558e-6
0.1	0	9.38991e-6	1.41917e-5	1.68401e-5	1.13680e-5	7.00631e-6	4.25867e-6
0.2	0	4.99787e-6	8.41462e-6	1.19931e-5	1.13331e-5	7.91561e-6	5.09952e-6
0.3	0	3.02141e-6	5.29147e-6	8.12382e-6	9.26819e-6	7.30285e-6	5.16014e-6
0.4	0	1.83088e-6	3.27241e-6	5.22780e-6	6.66903e-6	5.71842e-6	4.36413e-6
0.5	0	1.04255e-6	1.88668e-6	3.08937e-6	4.23874e-6	3.85640e-6	3.11870e-6
0.6	0	5.24606e-7	9.57346e-7	1.59419e-6	2.30167e-6	2.18631e-6	1.84705e-6
0.7	0	2.12804e-7	3.90688e-7	6.58548e-7	9.87231e-7	9.68785e-7	8.46476e-7
0.8	0	5.74705e-8	1.05990e-7	1.80314e-7	2.78220e-7	2.80038e-7	2.51273e-7
0.9	0	5.68457e-9	1.05210e-8	1.80285e-8	2.84596e-8	2.92330e-8	2.67986e-8
1.0	0	0	0	0	0	0	0

Table 11: Mie Scattering – The Fourier Component $I_*(\tau, \mu)$ for $m = 8$, with a computational time of approximately 0.026 seconds.

$\boldsymbol{\mu}$	$\boldsymbol{\tau = 0}$	$\boldsymbol{\tau = 0.05\tau_0}$	$\boldsymbol{\tau = 0.1\tau_0}$	$\boldsymbol{\tau = 0.2\tau_0}$	$\boldsymbol{\tau = 0.5\tau_0}$	$\boldsymbol{\tau = 0.75\tau_0}$	$\boldsymbol{\tau = \tau_0}$
-1.0	0	0	0	0	0	0	0
-0.9	6.56254e-10	5.89143e-10	5.28152e-10	4.22197e-10	1.99346e-10	8.28473e-11	0
-0.8	9.16369e-9	8.23263e-9	7.38637e-9	5.91575e-9	2.81653e-9	1.18325e-9	0
-0.7	4.02493e-8	3.61908e-8	3.25016e-8	2.60890e-8	1.25472e-8	5.34291e-9	0
-0.6	1.09663e-7	9.87034e-8	8.87413e-8	7.14229e-8	3.47818e-8	1.50704e-8	0
-0.5	2.29190e-7	2.06523e-7	1.85923e-7	1.50118e-7	7.42637e-8	3.29292e-8	0
-0.4	4.03647e-7	3.64199e-7	3.28368e-7	2.66136e-7	1.34335e-7	6.15090e-8	0
-0.3	6.29436e-7	5.68693e-7	5.13578e-7	4.18023e-7	2.16513e-7	1.03927e-7	0
-0.2	8.94476e-7	8.09046e-7	7.31658e-7	5.97914e-7	3.19414e-7	1.65053e-7	0
-0.1	1.18131e-6	1.06889e-6	9.67164e-7	7.91809e-7	4.33507e-7	2.50465e-7	0
-0.0	1.47573e-6	1.33530e-6	1.20823e-6	9.89214e-7	5.42893e-7	3.29281e-7	0
0.0	0	1.33530e-6	1.20823e-6	9.89214e-7	5.42893e-7	3.29281e-7	1.99719e-7
0.1	0	5.28593e-7	7.98899e-7	9.47982e-7	6.39936e-7	3.94403e-7	2.39731e-7
0.2	0	2.63292e-7	4.43289e-7	6.31803e-7	5.97029e-7	4.16994e-7	2.68642e-7
0.3	0	1.47638e-7	2.58560e-7	3.96958e-7	4.52873e-7	3.56839e-7	2.52139e-7
0.4	0	8.20707e-8	1.46688e-7	2.34338e-7	2.9894e-7	2.56328e-7	1.95622e-7
0.5	0	4.22497e-8	7.64582e-8	1.25197e-7	1.71775e-7	1.56280e-7	1.26385e-7
0.6	0	1.88253e-8	3.43539e-8	5.72066e-8	8.25936e-8	7.84537e-8	6.62795e-8
0.7	0	6.54561e-9	1.20171e-8	2.02561e-8	3.03658e-8	2.97984e-8	2.60363e-8
0.8	0	1.42836e-9	2.63425e-9	4.48146e-9	6.91474e-9	6.95991e-9	6.24498e-9
0.9	0	9.88569e-11	1.82964e-10	3.13522e-10	4.94919e-10	5.08367e-10	4.66032e-10
1.0	0	0	0	0	0	0	0

Furthermore, we ran the TFC algorithm by increasing the angle and spatial discretizations to achieve the 7-digit accuracy published by Ganapol [32] for $m = 0$. Our results are presented in Table 12. For those simulations, the following parameters have been employed: $N = 35$, $M = 300$, and $m = 90$. TFC has achieved the reported solutions with a computational time of 2.6 seconds. Conversely, for $m = 8$ Fourier component, the 7-digit accuracy of Ganapol have been achieved without the need to increase eitheer the angle or spatial discretization. Indeed, as in the previous case, the following parameters have been used: $N = 15$, $M = 100$, and $m = 40$. Results are shown in Table 13.

Table 12: Mie Scattering – The Fourier Component $I_*(\tau, \mu)$ for $m = 0$, according to Ganapol [32], with a computational time of approximately 2.6 seconds.

μ	$\tau = 0$	$\tau = 0.05\tau_0$	$\tau = 0.1\tau_0$	$\tau = 0.2\tau_0$	$\tau = 0.5\tau_0$	$\tau = 0.75\tau_0$	$\tau = \tau_0$
-1.0	4.7680739e-2	4.4191232e-2	4.0646720e-2	3.3709854e-2	1.5857241e-2	5.4529708e-3	0
-0.9	6.4564440e-2	6.0374289e-2	5.6013853e-2	4.7289947e-2	2.3812095e-2	9.0108349e-3	0
-0.8	8.4587655e-2	7.9676269e-2	7.4442518e-2	6.3753956e-2	3.3828695e-2	1.3691858e-2	0
-0.7	1.0834976e-1	1.0271869e-1	9.6567817e-2	8.3748795e-2	4.6491789e-2	1.9884482e-2	0
-0.6	1.3650449e-1	1.3020361e-1	1.2312760e-1	1.0806281e-1	6.2604846e-2	2.8172141e-2	0
-0.5	1.6967721e-1	1.6285165e-1	1.5491892e-1	1.3761804e-1	8.3292056e-2	3.9479159e-2	0
-0.4	2.0822991e-1	2.0120060e-1	1.9262576e-1	1.7335796e-1	1.1012425e-1	5.5363056e-2	0
-0.3	2.5167744e-1	2.4506518e-1	2.3630972e-1	2.1580644e-1	1.4514429e-1	7.8629773e-2	0
-0.2	2.9752321e-1	2.9240107e-1	2.8424081e-1	2.6379979e-1	1.9003527e-1	1.1455737e-1	0
-0.1	3.4012557e-1	3.3847566e-1	3.3198375e-1	3.1288756e-1	2.4121715e-1	1.7069703e-1	0
-0.0	3.5937904e-1	3.7448490e-1	3.7380021e-1	3.5934745e-1	2.8825763e-1	2.2562269e-1	0
0.0	0	3.7448490e-1	3.7380021e-1	3.5934745e-1	2.8825763e-1	2.2562269e-1	1.5152044e-1
0.1	0	1.5561969e-1	2.5142670e-1	3.3886425e-1	3.3070258e-1	2.6985545e-1	2.0307340e-1
0.2	0	9.2437025e-2	1.6508021e-1	2.6188673e-1	3.3551731e-1	3.0155334e-1	2.4424153e-1
0.3	0	6.7072588e-2	1.2414425e-1	2.1038294e-1	3.1480528e-1	3.0971262e-1	2.7030221e-1
0.4	0	5.3016958e-2	9.9893927e-2	1.7530448e-1	2.8818268e-1	3.0293863e-1	2.8106600e-1
0.5	0	4.3718197e-2	8.3238337e-2	1.4925136e-1	2.6130432e-1	2.8846360e-1	2.8082243e-1
0.6	0	3.6786430e-2	7.0519358e-2	1.2832314e-1	2.3525903e-1	2.6979273e-1	2.7302917e-1
0.7	0	3.1141106e-2	5.9990823e-2	1.1038662e-1	2.0993897e-1	2.4847557e-1	2.5982225e-1
0.8	0	2.6222496e-2	5.0716634e-2	9.4200130e-2	1.8498212e-1	2.2517903e-1	2.4245347e-1
0.9	0	2.1713290e-2	4.2153804e-2	7.9003938e-2	1.6003444e-1	2.0018674e-1	2.2166696e-1
1.0	0	1.7423141e-2	3.3971636e-2	6.4319263e-2	1.3481854e-1	1.7362739e-1	1.9793246e-1

Table 13: Mie Scattering – The Fourier Component $I_*(\tau, \mu)$ for $m = 8$, according to Ganapol [32], with a computational time of approximately 0.026 seconds.

μ	$\tau = 0$	$\tau = 0.05\tau_0$	$\tau = 0.1\tau_0$	$\tau = 0.2\tau_0$	$\tau = 0.5\tau_0$	$\tau = 0.75\tau_0$	$\tau = \tau_0$
-1.0	0	0	0	0	0	0	0
-0.9	6.5625391e-10	5.8914304e-10	5.2815237e-10	4.2219714e-10	1.9934608e-10	8.2847308e-11	0
-0.8	9.1636878e-9	8.2326319e-9	7.3863711e-9	5.9157513e-9	2.8165373e-9	1.1832473e-9	0
-0.7	4.0249326e-8	3.6190815e-8	3.2501619e-8	2.6088956e-8	1.2547246e-8	5.3429052e-9	0
-0.6	1.0966293e-7	9.8703386e-8	8.8741262e-8	7.1422850e-8	3.4781849e-8	1.5070373e-8	0
-0.5	2.2918971e-7	2.0652282e-7	1.8592286e-7	1.5011771e-7	7.4263736e-8	3.2929240e-8	0
-0.4	4.0364654e-7	3.6419928e-7	3.2836806e-7	2.6613595e-7	1.3433461e-7	6.1509004e-8	0
-0.3	6.2943646e-7	5.6869337e-7	5.1357757e-7	4.1802334e-7	2.1651285e-7	1.0392686e-7	0
-0.2	8.9447618e-7	8.0904612e-7	7.3165782e-7	5.9791370e-7	3.1941422e-7	1.6505266e-7	0
-0.1	1.1813127e-6	1.0688908e-6	9.6716367e-7	7.9180936e-7	4.3350657e-7	2.5046511e-7	0
-0.0	1.4757328e-6	1.3352990e-6	1.2082288e-6	9.8921442e-7	5.4289266e-7	3.2928109e-7	0
0.0	0	1.3352990e-6	1.2082288e-6	9.8921442e-7	5.4289266e-7	3.2928109e-7	1.9971892e-7
0.1	0	5.2859344e-7	7.9889942e-7	9.4798249e-7	6.3993602e-7	3.9440254e-7	2.3973118e-7
0.2	0	2.6329242e-7	4.4328927e-7	6.3180326e-7	5.9702947e-7	4.1699385e-7	2.6864210e-7
0.3	0	1.4763750e-7	2.5856043e-7	3.9695812e-7	4.5287275e-7	3.5683886e-7	2.5213926e-7
0.4	0	8.2070715e-8	1.4668783e-7	2.3433850e-7	2.9894033e-7	2.5632829e-7	1.9562189e-7
0.5	0	4.2249686e-8	7.6458207e-8	1.2519740e-7	1.7177455e-7	1.5627982e-7	1.2638468e-7
0.6	0	1.8825271e-8	3.4353900e-8	5.7206557e-8	8.2593552e-8	7.8453748e-8	6.6279496e-8
0.7	0	6.5456093e-9	1.2017087e-8	2.0256111e-8	3.0365796e-8	2.9798350e-8	2.6036280e-8
0.8	0	1.4283575e-9	2.6342575e-9	4.4814591e-9	6.9147374e-9	6.9599115e-9	6.2449834e-9
0.9	0	9.8856917e-11	1.8296411e-10	3.1352189e-10	4.9491896e-10	5.0836713e-10	4.6603207e-10
1.0	0	0	0	0	0	0	0

For the Haze L problem, which was posed as a basic test problem by the Radiation Commission of the International Association of Meteorology and Atmospheric Physics (IAMAP) [33], we compared our results with the ones reported in [27] and [31]. In such cases, the authors used an angular discretization of $N = 100 - 150$. For all our simulations, we ran the TFC algorithm with a discretization of $N = 30$. The same parameters, as reported below, are used in all cases. An exception is represented by the parameter m, which is varied across cases. The one–angle case, when the incident beam direction is $\mu_0 = 1$, requires to compute only the 1^{st} Fourier component $m = 0$, i.e. without considering the azimuthal angle. In the two–angle cases,

we calculated all the $L+1$ Fourier components. The TFC results are reported in tables 14 - 18.
For the normal incidence case, the following parameters have been used: $N = 30$, $M = 250$, $m_{op} = 90$, $\tau_0 = 1$, $S_0 = 1$, $\mu_0 = 1$, $\omega = 0.9$. For the conservative case, the following parameters have been used: $N = 30$, $M = 250$, $m_{op} = 90$, $\tau_0 = 1$, $S_0 = 1$, $\mu_0 = 1$, $\omega = 1$. For both simulations, the computational times are approximately 1.6 seconds.
For the two-angle case, the incident beam is not $\mu_0 = 1$, so we needed to compute all the $L+1$ Fourier components. For the Haze L problem, 83 components are required. However, we found out that it was not necessary to modify the parameters for each case. The three different cases are reported below:

1) $\phi - \phi_0 = 0$,

2) $\phi - \phi_0 = \pi/2$,

3) $\phi - \phi_0 = \pi$.

The set of parameters used was: $N = 30$, $M = 250$, $m_{op} = 90$, $\tau_0 = 1$, $S_0 = 1$, $\mu_0 = 0.5$, $\omega = 0.9$. The TFC computational time is reported to be approximately 132 seconds. Even in this case we were able to obtain all the digits published by Siewert et al. [27, 31].

Table 14: Haze L Problem - The Intensity $I_*(\tau, \mu)$ for the Haze L phase function with $\omega = 0.9$ and $\mu_0 = 1$, with a computational time of approximately 1.6 seconds.

$\boldsymbol{\mu}$	$\boldsymbol{\tau = 0}$	$\boldsymbol{\tau = 0.05\tau_0}$	$\boldsymbol{\tau = 0.1\tau_0}$	$\boldsymbol{\tau = 0.2\tau_0}$	$\boldsymbol{\tau = 0.5\tau_0}$	$\boldsymbol{\tau = 0.75\tau_0}$	$\boldsymbol{\tau = \tau_0}$
-1.0	2.79717e-2	2.65834e-2	2.51795e-2	2.23421e-2	1.37519e-2	6.70439e-3	0
-0.9	3.01802e-2	2.87427e-2	2.72763e-2	2.42824e-2	1.50370e-2	7.32793e-3	0
-0.8	3.14478e-2	3.00707e-2	2.86411e-2	2.56621e-2	1.60962e-2	7.85504e-3	0
-0.7	3.43839e-2	3.30557e-2	3.16407e-2	2.86060e-2	1.83142e-2	9.00263e-3	0
-0.6	3.91308e-2	3.78910e-2	3.65135e-2	3.34278e-2	2.20977e-2	1.10619e-2	0
-0.5	4.56379e-2	4.46171e-2	4.33840e-2	4.04032e-2	2.80086e-2	1.45143e-2	0
-0.4	5.35113e-2	5.29854-2	5.21410e-2	4.96862e-2	3.68540e-2	2.02308e-2	0
-0.3	6.15420e-2	6.19914e-2	6.19786e-2	6.08863e-2	4.96165e-2	2.98277e-2	0
-0.2	6.69562e-2	6.90564e-2	7.04996e-2	7.20372e-2	6.66970e-2	4.63006e-2	0
-0.1	6.55296e-2	7.00041e-2	7.34324e-2	7.85904e-2	8.44628e-2	7.36110e-2	0
-0.0	5.17485e-2	6.17096e-2	6.80163e-2	7.74665e-2	9.39979e-2	9.74837e-2	0
0.0	0	6.17096e-2	6.80163e-2	7.74665e-2	9.39978e-2	9.74837e-2	7.93126e-2
0.1	0	2.24949e-2	3.95181e-2	6.26530e-2	9.62543e-2	1.08718e-1	1.08189e-1
0.2	0	1.31007e-2	2.53401e-2	4.67729e-2	9.15916e-2	1.13815e-1	1.24212e-1
0.3	0	1.01943e-2	2.02703e-2	3.94722e-2	8.74675e-2	1.16620e-1	1.35712e-1
0.4	0	9.52906e-3	1.90677e-2	3.77703e-2	8.83323e-2	1.22503e-1	1.48268e-1
0.5	0	1.02637e-2	2.05023e-2	4.06492e-2	9.64183e-2	1.35817e-1	1.67516e-1
0.6	0	1.25293e-2	2.49095e-2	4.90656e-2	1.15336e-1	1.62230e-1	2.00701e-1
0.7	0	1.74171e-2	3.44152e-2	6.70811e-2	1.53982e-1	2.13563e-1	2.61672e-1
0.8	0	2.85622e-2	5.60204e-2	1.07697e-2	2.38486e-1	3.22550e-1	3.86921e-1
0.9	0	6.16331e-2	1.19763e-1	2.26124e-1	4.76103e-1	6.19703e-1	7.17745e-1
1.0	0	3.28124e-1	6.29065e-1	1.15632	2.24839	2.74147	2.97766

Table 15: Haze L Problem - The Intensity $I_*(\tau, \mu)$ for the Haze L phase function with $\omega = 1$ and $\mu_0 = 1$, with a computational time of approximately 1.6 seconds.

$\boldsymbol{\mu}$	$\boldsymbol{\tau = 0}$	$\boldsymbol{\tau = 0.05\tau_0}$	$\boldsymbol{\tau = 0.1\tau_0}$	$\boldsymbol{\tau = 0.2\tau_0}$	$\boldsymbol{\tau = 0.5\tau_0}$	$\boldsymbol{\tau = 0.75\tau_0}$	$\boldsymbol{\tau = \tau_0}$
-1.0	3.61452e-2	3.43394e-2	3.25109e-2	2.88122e-2	1.76286e-2	8.52589e-3	0
-0.9	3.97819e-2	3.78723e-2	3.59207e-2	3.19303e-2	1.96202e-2	9.45731e-3	0
-0.8	4.27313e-2	4.08406e-2	3.88734e-2	3.47677e-2	2.16019e-2	1.03959e-2	0
-0.7	4.80051e-2	4.61319e-2	4.41307e-2	3.98292e-2	2.52479e-2	1.22171e-2	0
-0.6	5.58214e-2	5.40432e-2	5.20594e-2	4.75986e-2	3.11837e-2	1.53618e-2	0
-0.5	6.60942e-2	6.46296e-2	6.28449e-2	5.84971e-2	4.02740e-2	2.05621e-2	0
-0.4	7.81481e-2	7.74403e-2	7.62508e-2	7.27049e-2	5.37300e-2	2.91285e-2	0
-0.3	8.99682e-2	9.07706e-2	9.08784e-2	8.94711e-2	7.29643e-2	4.34688e-2	0
-0.2	9.70815e-2	1.00421e-1	1.02789e-1	1.05506e-1	9.83777e-2	6.79949e-2	0
-0.1	9.29328e-2	9.98187e-2	1.05195e-1	1.13497e-1	1.24037e-1	1.08399e-2	0
-0.0	6.98774e-2	8.46673e-2	9.41663e-1	1.08727e-1	1.35762e-1	1.42779e-1	0
0.0	0	8.46673e-2	9.41663e-1	1.08727e-1	1.35762e-1	1.42779e-1	1.14808e-1
0.1	0	2.95418e-2	5.24346e-2	8.45649e-2	1.35096e-1	1.56106e-1	1.56976-1
0.2	0	1.64907e-2	3.22817e-2	6.07527e-2	1.24350e-1	1.58925e-1	1.76818e-1
0.3	0	1.23421e-2	2.48488e-2	4.93968e-2	1.14811e-1	1.57937e-1	1.88301e-1
0.4	0	1.11879e-2	2.26450e-2	4.57547e-2	1.12269e-1	1.60862e-1	2.00019e-1
0.5	0	1.17959e-2	2.37910e-2	4.80003e-2	1.19079e-1	1.73191e-1	2.19633e-1
0.6	0	1.42049e-2	2.84584e-2	5.68731e-2	1.39051e-1	2.01445e-1	2.55983e-1
0.7	0	1.95833e-2	3.89248e-2	7.67454e-2	1.82004e-1	2.58986e-1	3.25125e-1
0.8	0	3.19532e-2	6.29430e-2	1.22045e-1	2.77182e-1	3.82767e-1	4.68658e-1
0.9	0	6.87267e-2	1.33917e-1	2.54259e-1	5.44601e-1	7.19447e-1	8.46084e-1
1.0	0	3.64940e-1	7.00266e-1	1.28955	2.52255	3.09319	3.38091

Table 16: Haze L Problem - The Intensity $I_*(\tau, \mu, \phi)$ for the Haze L phase function with $\omega = 0.9$, $\mu_0 = 0.5$, and $\phi - \phi_0 = 0$, with a computational time of approximately 132 seconds.

$\boldsymbol{\mu}$	$\boldsymbol{\tau = 0}$	$\boldsymbol{\tau = 0.05\tau_0}$	$\boldsymbol{\tau = 0.1\tau_0}$	$\boldsymbol{\tau = 0.2\tau_0}$	$\boldsymbol{\tau = 0.5\tau_0}$	$\boldsymbol{\tau = 0.75\tau_0}$	$\boldsymbol{\tau = \tau_0}$
-1.0	2.28190e-2	2.14170e-2	1.99920e-2	1.71574e-2	9.34719e-3	4.02513e-3	0
-0.9	4.11125e-2	3.86276e-2	3.60559e-2	3.08703e-2	1.64542e-2	6.81049e-3	0
-0.8	6.49983e-2	6.12972e-2	5.73958e-2	4.94000e-2	2.66078e-2	1.10213e-2	0
-0.7	9.99446e-2	9.47422e-2	8.91210e-2	7.73509e-2	4.26132e-2	1.79328e-2	0
-0.6	1.50993e-1	1.44083e-1	1.36343e-1	1.19657e-1	6.81169e-2	2.95065e-2	0
-0.5	2.24768e-1	2.16263e-1	2.06169e-1	1.83479e-1	1.09068e-1	4.93125e-2	0
-0.4	3.29336e-1	3.20182e-1	3.08045e-1	2.78889e-1	1.75210e-1	8.41056e-2	0
-0.3	4.72536e-1	4.65520e-1	4.52954e-1	4.18719e-1	2.82082e-1	1.47239e-1	0
-0.2	6.56834e-1	6.58390e-1	6.49495e-1	6.15206e-1	4.51466e-1	2.66183e-1	0
-0.1	8.70325e-1	8.94525e-1	8.97446e-1	8.72172e-1	6.97514e-1	4.91555e-1	0
-0.0	1.03177	1.14775	1.18797	1.19440	1.00873	7.95748e-1	0
0.0	0	1.14775	1.18797	1.19440	1.00873	7.95748e-1	5.24167e-1
0.1	0	6.07548e-1	9.98592e-1	1.38473	1.41181	1.15806	8.76470e-1
0.2	0	5.08883e-1	9.07223e-1	1.43790	1.82630	1.61273	1.29144
0.3	0	5.49994e-1	9.99898e-1	1.64825	2.30787	2.15587	1.80549
0.4	0	6.38615e-1	1.16925	1.95778	2.87301	2.77822	2.40104
0.5	0	6.34271e-1	1.16869	1.98321	3.03333	3.03426	2.71055
0.6	0	4.18260e-1	7.78087e-1	1.34620	2.18395	2.29506	2.15369
0.7	0	2.04883e-1	3.85810e-1	6.83932e-1	1.19334	1.33200	1.32682
0.8	0	8.64752e-2	1.65150e-1	3.01013e-1	5.69583e-1	6.78608e-1	7.19934e-1
0.9	0	3.13664e-2	6.09010e-2	1.14612e-1	2.37335e-1	3.03207e-1	3.43478e-1
1.0	0	5.07113e-3	1.01191e-2	2.00435e-2	4.76083e-2	6.73492e-2	8.37579e-2

Table 17: Haze L Problem - The Intensity $I_*(\tau, \mu, \phi)$ for the Haze L phase function with $\omega = 0.9$, $\mu_0 = 0.5$, and $\phi - \phi_0 = \pi/2$, with a computational time of approximately 132 seconds.

$\boldsymbol{\mu}$	$\boldsymbol{\tau = 0}$	$\boldsymbol{\tau = 0.05\tau_0}$	$\boldsymbol{\tau = 0.1\tau_0}$	$\boldsymbol{\tau = 0.2\tau_0}$	$\boldsymbol{\tau = 0.5\tau_0}$	$\boldsymbol{\tau = 0.75\tau_0}$	$\boldsymbol{\tau = \tau_0}$
-1.0	2.28190e-2	2.14170e-2	1.99920e-2	1.71574e-2	9.34719e-3	4.02513e-3	0
-0.9	2.69861e-2	2.54001e-2	2.3770e-2	2.04885e-2	1.12507e-2	4.83998e-3	0
-0.8	3.23251e-2	3.05433e-2	2.86841e-2	2.48816e-2	1.38576e-2	5.98687e-3	0
-0.7	3.90915e-2	3.71288e-2	3.50364e-2	3.06624e-2	1.74617e-2	7.63435e-3	0
-0.6	4.75194e-2	4.54446e-2	4.31587e-2	3.82274e-2	2.24929e-2	1.00585e-2	0
-0.5	5.76960e-2	5.56800e-2	5.33274e-2	4.79966e-2	2.95696e-2	1.37243e-2	0
-0.4	6.92921e-2	6.76843e-2	6.55506e-2	6.02592e-2	3.95485e-2	1.94423e-2	0
-0.3	8.09723e-2	8.04082e-2	7.90373e-2	7.47154e-2	5.34553e-2	2.86762e-2	0
-0.2	8.94088e-2	9.08993e-2	9.11597e-2	8.93864e-2	7.18225e-2	4.41114e-2	0
-0.1	8.86327e-2	9.36078e-2	9.65669e-2	9.91642e-2	9.15413e-2	6.94491e-2	0
-0.0	6.76014e-2	8.16018e-2	8.92220e-2	9.83762e-2	1.03484e-1	9.32369e-2	0
0.0	0	8.16018e-2	8.92220e-2	9.83762e-2	1.03484e-1	9.32371e-2	6.29164e-2
0.1	0	2.74475e-2	4.83619e-2	7.57571e-2	1.04622e-1	1.04387e-1	8.95907e-2
0.2	0	1.41330e-2	2.75945e-2	5.09061e-2	9.28868e-2	1.04678e-1	1.01178e-1
0.3	0	9.26644e-3	1.87294e-2	3.68737e-2	7.85470e-2	9.74004e-2	1.02990e-1
0.4	0	6.96644e-3	1.42411e-2	2.88244e-2	6.68034e-2	8.82947e-2	9.95180e-2
0.5	0	5.75720e-3	1.17847e-2	2.40718e-2	5.82338e-2	8.01154e-2	9.43192e-2
0.6	0	5.11030e-3	1.04251e-2	2.12819e-2	5.23831e-2	7.37544e-2	8.93298e-2
0.7	0	4.79703e-3	9.73440e-3	1.97631e-2	4.87196e-2	6.93677e-2	8.54626e-2
0.8	0	4.71115e-3	9.50506e-3	1.91501e-2	4.68396e-2	6.68825e-2	8.31200e-2
0.9	0	4.80640e-3	9.64244e-3	1.92635e-2	4.64998e-2	6.62130e-2	8.24990e-2
1.0	0	5.07113e-3	1.01191e-2	2.00435e-2	4.76083e-2	6.73492e-2	8.37579e-2

Table 18: Haze L Problem - The Intensity $I_*(\tau, \mu, \phi)$ for the Haze L phase function with $\omega = 0.9$, $\mu_0 = 0.5$, and $\phi - \phi_0 = \pi$, with a computational time of approximately 132 seconds.

$\boldsymbol{\mu}$	$\boldsymbol{\tau = 0}$	$\boldsymbol{\tau = 0.05\tau_0}$	$\boldsymbol{\tau = 0.1\tau_0}$	$\boldsymbol{\tau = 0.2\tau_0}$	$\boldsymbol{\tau = 0.5\tau_0}$	$\boldsymbol{\tau = 0.75\tau_0}$	$\boldsymbol{\tau = \tau_0}$
-1.0	2.28190e-2	2.14170e-2	1.99920e-2	1.71574e-2	9.34719e-3	4.02513e-3	0
-0.9	2.61852e-2	2.46217e-2	2.30415e-2	1.99042e-2	1.11589e-2	4.97196e-3	0
-0.8	3.20368e-2	3.01730e-2	2.82831e-2	2.45151e-2	1.38928e-2	6.24448e-3	0
-0.7	3.74817e-2	3.54358e-2	3.33331e-2	2.90811e-2	1.67591e-2	7.61010e-3	0
-0.6	4.12139e-2	3.92700e-2	3.72011e-2	3.28685e-2	1.95280e-2	9.02300e-3	0
-0.5	4.99464e-2	4.77799e-2	4.54343e-2	4.04517e-2	2.46595e-2	1.16636e-2	0
-0.4	5.50134e-2	5.32394e-2	5.11567e-2	4.64342e-2	2.98815e-2	1.47743e-2	0
-0.3	6.44934e-2	6.30132e-2	6.10801e-2	5.64129e-2	3.85985e-2	2.04385e-2	0
-0.2	7.08868e-2	7.03673e-2	6.91450e-2	6.55321e-2	4.91145e-2	2.92042e-2	0
-0.1	6.95600e-2	7.10895e-2	7.13778e-2	7.01215e-2	5.90302e-2	4.25269e-2	0
-0.0	5.47761e-2	6.23325e-2	6.55280e-2	6.81201e-2	6.39396e-2	5.39412e-2	0
0.0	0	6.23325e-2	6.55280e-2	6.81201e-2	6.39396e-2	5.39412e-2	3.42189e-2
0.1	0	1.99925e-2	3.42555e-2	5.10066e-2	6.25009e-2	5.80166e-2	4.66801e-2
0.2	0	9.41145e-3	1.79861e-2	3.18930e-2	5.27234e-2	5.56537e-2	5.06958e-2
0.3	0	5.52988e-3	1.10120e-2	2.10538e-2	4.15040e-2	4.87980e-2	4.91257e-2
0.4	0	3.67310e-3	7.45174e-3	1.48051e-2	3.24697e-2	4.12526e-2	4.48014e-2
0.5	0	2.67314e-3	5.46407e-3	1.10690e-2	2.59261e-2	3.47946e-2	3.99910e-2
0.6	0	2.11016e-3	4.31933e-3	8.82241e-3	2.14934e-2	2.99722e-2	3.59328e-2
0.7	0	1.81107e-3	3.69988e-3	7.56877e-3	1.88391e-2	2.69599e-2	3.33330e-2
0.8	0	1.72244e-3	3.50577e-3	7.15364e-3	1.79613e-2	2.61129e-2	3.29719e-2
0.9	0	1.93240e-3	3.91318e-3	7.93848e-3	1.98733e-2	2.90534e-2	3.70748e-2
1.0	0	5.07113e-3	1.01191e-2	2.00435e-2	4.76083e-2	6.73492e-2	8.37579e-2

Again, we increased the TFC angular and spatial discretizations to improve the accuracy of the solutions, and to achieve the 7-digit accuracy as published by Ganapol for the Haze L problem. We computed the

incident cases ($\mu_0 = 1$), with both conservative single scattering albedo $\omega = 1$ and non-conservative single scattering albedo $\omega = 0.9$. We found that the optimal parameters are $N = 35$, $M = 400$, and $m_{op} = 100$. The TFC computational time is reported to be approximately 4.4 seconds. The results are reported in Tables 19 and 20.

Table 19: Haze L Problem - The Intensity $I_*(\tau, \mu)$ for the Haze L phase function with $\omega = 0.9$ and $\mu_0 = 1$, according to Ganapol [32], with a computational time of approximately 4.4 seconds.

$\boldsymbol{\mu}$	$\boldsymbol{\tau = 0}$	$\boldsymbol{\tau = 0.05\tau_0}$	$\boldsymbol{\tau = 0.1\tau_0}$	$\boldsymbol{\tau = 0.2\tau_0}$	$\boldsymbol{\tau = 0.5\tau_0}$	$\boldsymbol{\tau = 0.75\tau_0}$	$\boldsymbol{\tau = \tau_0}$
-1.0	2.7971665e-2	2.6583431e-2	2.5179489e-2	2.2342144e-2	1.3751918e-2	6.7043863e-3	0
-0.9	3.0180197e-2	2.8742728e-2	2.7276328e-2	2.4282402e-2	1.5036989e-2	7.3279307e-3	0
-0.8	3.1447755e-2	3.0070750e-2	2.8641094e-2	2.5662054e-2	1.6096218e-2	7.8550379e-3	0
-0.7	3.4383906e-2	3.3055747e-2	3.1640694e-2	2.8605980e-2	1.8314210e-2	9.0026264e-3	0
-0.6	3.9130810e-2	3.7890987e-2	3.6513506e-2	3.3427829e-2	2.2097749e-2	1.1061916e-2	0
-0.5	4.5637920e-2	4.4617111e-2	4.3383966e-2	4.0403191e-2	2.8008565e-2	1.4514343e-2	0
-0.4	5.3511337e-2	5.2985449e-2	5.2140980e-2	4.9686294e-2	3.6854018e-2	2.0230769e-2	0
-0.3	6.1542012e-2	6.1991418e-2	6.1978635e-2	6.0886294e-2	4.9616521e-2	2.9827680e-2	0
-0.2	6.6956243e-2	6.9056402e-2	7.0499635e-2	7.2037240e-2	6.6696988e-2	4.6300639e-2	0
-0.1	6.5529583e-2	7.0004105e-2	7.3432378e-2	7.8590386e-2	8.4462845e-2	7.3611021e-2	0
-0.0	5.1748534e-2	6.1709609e-2	6.8016336e-2	7.7466538e-2	9.3997859e-2	9.7483668e-2	0
0.0	0	6.1709609e-2	6.8016336e-2	7.7466538e-2	9.3997859e-2	9.7483668e-2	7.9312594e-2
0.1	0	2.2494931e-2	3.9518122e-2	6.2652973e-2	9.6254337e-2	1.0871841e-1	1.0818930e-1
0.2	0	1.3100677e-2	2.5340076e-2	4.6772905e-2	9.1591615e-2	1.1381468e-1	1.2421167e-1
0.3	0	1.0194331e-2	2.0270341e-2	3.9472225e-2	8.7467481e-2	1.1662007e-1	1.3571209e-1
0.4	0	9.5290644e-3	1.9067650e-2	3.7770256e-2	8.8332315e-2	1.2250259e-1	1.4826767e-1
0.5	0	1.0263750e-2	2.0502330e-2	4.0649220e-2	9.6418345e-2	1.3581653e-1	1.6751584e-1
0.6	0	1.2529327e-2	2.4909477e-2	4.9065634e-2	1.1533634e-1	1.6223048e-1	2.0070062e-1
0.7	0	1.7417124e-2	3.4415206e-2	6.7081148e-2	1.5398186e-1	2.1356335e-1	2.6167192e-1
0.8	0	2.8562211e-2	5.6020429e-2	1.0769702e-2	2.3848565e-1	3.2254956e-1	3.8692070e-1
0.9	0	6.1633112e-2	1.1976311e-1	2.2612375e-1	4.7610276e-1	6.1970346e-1	7.1774509e-1
1.0	0	3.2812354e-1	6.2906510e-1	1.1563161	2.2483946	2.7414726	2.9776602

Table 20: Haze L Problem - The Intensity $I_*(\tau, \mu)$ for the Haze L phase function with $\omega = 1$ and $\mu_0 = 1$, according to Ganapol [32], with a computational time of approximately 4.4 seconds.

$\boldsymbol{\mu}$	$\boldsymbol{\tau = 0}$	$\boldsymbol{\tau = 0.05\tau_0}$	$\boldsymbol{\tau = 0.1\tau_0}$	$\boldsymbol{\tau = 0.2\tau_0}$	$\boldsymbol{\tau = 0.5\tau_0}$	$\boldsymbol{\tau = 0.75\tau_0}$	$\boldsymbol{\tau = \tau_0}$
-1.0	3.6145156e-2	3.4339396e-2	3.2510866e-2	2.8812216e-2	1.7628611e-2	8.5258908e-3	0
-0.9	3.9781870e-2	3.7872320e-2	3.5920682e-2	3.1930313e-2	1.9620173e-2	9.4573134e-3	0
-0.8	4.2731263e-2	4.0840607e-2	3.8873442e-2	3.4767734e-2	2.1601856e-2	1.0395857e-2	0
-0.7	4.8005147e-2	4.6131929e-2	4.4130697e-2	3.9829198e-2	2.5247889e-2	1.2217079e-2	0
-0.6	5.5821353e-2	5.4043177e-2	5.2059351e-2	4.7598583e-2	3.1183660e-2	1.5361836e-2	0
-0.5	6.6094221e-2	6.4629636e-2	6.2844874e-2	5.8497071e-2	4.0273976e-2	2.0562127e-2	0
-0.4	7.8148081e-2	7.7440255e-2	7.6250769e-2	7.2704873e-2	5.3729974e-2	2.9128534e-2	0
-0.3	8.9968154e-2	9.0770642e-2	9.0878384e-2	8.9471128e-2	7.2964349e-2	4.3468799e-2	0
-0.2	9.7081540e-2	1.0042085e-1	1.0278927e-1	1.0550594e-1	9.8377715e-2	6.7994924e-2	0
-0.1	9.2932814e-2	9.9818714e-2	1.0519502e-1	1.1349749e-1	1.2403692e-1	1.0839912e-2	0
-0.0	6.9877391e-2	8.4667310e-2	9.4166299e-1	1.0872694e-1	1.3576248e-1	1.4277947e-1	0
0.0	0	8.4667310e-2	9.4166299e-1	1.0872694e-1	1.3576248e-1	1.4277947e-1	1.1480771e-1
0.1	0	2.9541820e-2	5.2434564e-2	8.4564915e-2	1.3509602e-1	1.5610649e-1	1.5697621-1
0.2	0	1.6490681e-2	3.2281653e-2	6.0752687e-2	1.2435036e-1	1.5892546e-1	1.7681766e-1
0.3	0	1.2342100e-2	2.4848764e-2	4.9396789e-2	1.1481121e-1	1.5793652e-1	1.8830112e-1
0.4	0	1.1187938e-2	2.2644991e-2	4.5754673e-2	1.1226864e-1	1.6086203e-1	2.0001870e-1
0.5	0	1.1795943e-2	2.3790964e-2	4.8000306e-2	1.1907946e-1	1.7319074e-1	2.1963289e-1
0.6	0	1.4204907e-2	2.8458379e-2	5.6873102e-2	1.3905102e-1	2.0144487e-1	2.5598334e-1
0.7	0	1.9583294e-2	3.8924848e-2	7.6745368e-2	1.8200357e-1	2.5898644e-1	3.2512495e-1
0.8	0	3.1953231e-2	6.2942983e-2	1.2204484e-1	2.7718191e-1	3.8276705e-1	4.6865779e-1
0.9	0	6.8726703e-2	1.3391677e-1	2.5425935e-1	5.4460066e-1	7.1944669e-1	8.4608373e-1
1.0	0	3.6493954e-1	7.0026634e-1	1.2895497	2.5225517	3.0931861	3.3809098

7. Conclusions and future outlooks

This paper highlights the potential of the *Theory of Functional Connections* to solve one-dimensional, anisotropic Radiative Transfer Problems in homogeneous media, with high accuracy for both one angle and

two angles incident source beam, at least up to the 7^{th} figure.
The advantage of the proposed method lies in its elegant and concise implementation, in the analytically satisfaction of boundary conditions, as well as in the absence of numerical issues for the conservative case ($\omega = 1$), and in the ability to compute the photon flux in any exact query spatial and directional points without further manipulations.
Moreover, it has been shown that via TFC, one is able to directly solve the Radiative Transfer Equation in the form of Eq. (38), without further transformations on the equation itself as usually necessary in other methods [16, 32]. Future works will focus on the application of the TFC to the Matrix Riccati Equation (MRE) solution of the 1D RTE arising from the application of the interaction principle of particle transport to Eq. (38) [34]. Indeed, using the MRE would allow us to tackle the problem via recursively applying the TFC method as presented in [22] for problems with a long integration space (e.g., τ for our case). Furthermore, we believe that this approach will allow us to combine the TFC methodology with the adding-doubling method proposed by Ganapol in [35, 36, 37, 38], in synergy with the Wynn-Epsilon Convergence Acceleration to further improve the performance of the TFC framework in solving even more challenging Radiative Transfer problems, such as the Cloud C1 problem, posed by IAMAP [33]. This benchmark requires a large optical depth ($\tau_0 = 64$). This is causing the matrix to invert to be large. Thus the problem becomes too computationally expensive both in terms of memory and computational time. Hence, at this stage, large optical depth is still the limitation of our proposed method. Indeed, while our TFC based method for solving the RTE is comparable with the other state of the art methods in tackling problems with small optical depths (e.g., Mie Scattering and Haze L problems), it appears to suffer when solving problems with large ones.
Additionally, future works will focus on the application of the newly developed *Extreme Theory of Functional Connections* (X-TFC) [39], that is a Physics-Informed Neural Network framework, to tackle some of the most challenging Radiative Transfer problems such as multi-slab case [40], time-dependent integrodifferential Boltzmann Equations, and, subsequently, 3D time-dependent Radiative Transfer Problems. Moreover, the application of X-TFC to time-dependent radiative transfer problems would aim to offer an alternative to the existing frameworks based on spectral and collocation methods such as [41, 42, 43]. We are currently applying the X-TFC physics-informed framework in solving a series of Rarefied-Gas Dynamics problems such as Poiseuille Flow and Thermal Creep Flow in a plane channel. Extension of the X-TFC to multi-dimensional RTEs is expected to be relatively straightforward.

References

[1] S. Chandrasekhar, *Radiative transfer*. Courier Corporation, 2013.

[2] G. C. Wick, "Über ebene diffusionsprobleme," *Zeitschrift für Physik*, vol. 121, no. 11-12, pp. 702–718, 1943.

[3] B. Carlson and G. Bell, "Solution of the transport equation by the Sn method," tech. rep., Los Alamos Scientific Lab., N. Mex., 1958.

[4] M. Vilhena, C. Segatto, and L. Barichello, "A particular solution for the sn radiative transfer problems," *Journal of Quantitative Spectroscopy and Radiative Transfer*, vol. 53, no. 4, pp. 467–469, 1995.

[5] K.-Y. Chien, "Application of the s, method to spherically symmetric radiative-transfer problems," *AIAA Journal*, vol. 10, no. 1, pp. 55–59, 1972.

[6] M. Simch, C. Segatto, and M. Vilhena, "An analytical solution for the sn radiative transfer equation with polarization in a slab by the ltsn method," *Journal of Quantitative Spectroscopy and Radiative Transfer*, vol. 97, no. 3, pp. 424–435, 2006.

[7] P. Benoist and A. Kavenoky, "A new method of approximation of the boltzmann equation," *Nuclear Science and Engineering*, vol. 32, no. 2, pp. 225–232, 1968.

[8] C. Siewert and P. Benoist, "The fn method in neutron-transport theory. part i: Theory and applications," *Nuclear Science and Engineering*, vol. 69, no. 2, pp. 156–160, 1979.

[9] C. Devaux and C. Siewert, "Thef n method for radiative transfer problems without azimuthal symmetry," *Zeitschrift für angewandte Mathematik und Physik ZAMP*, vol. 31, no. 5, pp. 592–604, 1980.

[10] R. Garcia and C. Siewert, "The fn method for radiative transfer models that include polarization effects," *Journal of Quantitative Spectroscopy and Radiative Transfer*, vol. 41, no. 2, pp. 117–145, 1989.

[11] B. D. Ganapol and R. Myneni, "The fn method for the one-angle radiative transfer equation applied to plant canopies," *Remote sensing of environment*, vol. 39, no. 3, pp. 213–231, 1992.

[12] M. Benassi, R. Cotta, and C. Siewert, "The PN method for radiative transfer problems with reflective boundary conditions," *Journal of Quantitative Spectroscopy and Radiative Transfer*, vol. 30, no. 6, pp. 547–553, 1983.

[13] M. Benassi, R. Garcia, A. Karp, and C. Siewert, "A high-order spherical harmonics solution to the standard problem in radiative transfer," *The Astrophysical Journal*, vol. 280, pp. 853–864, 1984.

[14] C. Siewert and J. Thomas Jr, "A particular solution for the pn method in radiative transfer," *Journal of Quantitative Spectroscopy and Radiative Transfer*, vol. 43, no. 6, pp. 433–436, 1990.

[15] L. Barichello and C. E. Siewert, "A discrete-ordinates solution for a non-grey model with complete frequency redistribution," *Journal of Quantitative Spectroscopy and Radiative Transfer*, vol. 62, no. 6, pp. 665–675, 1999.

[16] C. Siewert, "A concise and accurate solution to Chandrasekhar's basic problem in radiative transfer," *Journal of Quantitative Spectroscopy and Radiative Transfer*, vol. 64, no. 2, pp. 109–130, 2000.

[17] P. Picca and R. Furfaro, "Analytical discrete ordinate method for radiative transfer in dense vegetation canopies," *Journal of Quantitative Spectroscopy and Radiative Transfer*, vol. 118, pp. 60–69, 2013.

[18] B. Ganapol, "Radiative transfer with internal reflection via the converged discrete ordinates method," *Journal of Quantitative Spectroscopy and Radiative Transfer*, vol. 112, no. 4, pp. 693–713, 2011.

[19] P. Picca, R. Furfaro, and B. D. Ganapol, "An efficient multiproblem strategy for accurate solutions of linear particle transport problems in spherical geometry," *Nuclear science and engineering*, vol. 170, no. 2, pp. 103–124, 2012.

[20] D. Mortari, "The theory of connections: Connecting points," *Mathematics*, vol. 5, no. 4, p. 57, 2017.

[21] D. Mortari, "Least-squares solution of linear differential equations," *Mathematics*, vol. 5, no. 4, p. 48, 2017.

[22] D. Mortari, H. Johnston, and L. Smith, "High accuracy least-squares solutions of nonlinear differential equations," *Journal of Computational and Applied Mathematics*, vol. 352, pp. 293–307, 2019.

[23] R. Furfaro and D. Mortari, "Least-squares solution of a class of optimal space guidance problems via Theory of Connections," *Acta Astronautica*, 2019.

[24] H. Johnston, E. Schiassi, R. Furfaro, and D. Mortari, "Fuel-Efficient Powered Descent Guidance on Large Planetary Bodies via Theory of Functional Connections," *arXiv preprint arXiv:2001.03572*, 2020.

[25] E. Schiassi, A. D'Ambrosio, H. Johnston, R. Furfaro, F. Curti, and D. Mortari, "Complete Energy Optimal Landing on Planetary Bodies via Theory of Functional Connections," *Acta Astronautica - in preparation*, 2020.

[26] W. Meador and W. Weaver, "Two-stream approximations to radiative transfer in planetary atmospheres: A unified description of existing methods and a new improvement," *Journal of the atmospheric sciences*, vol. 37, no. 3, pp. 630–643, 1980.

[27] M. Benassi, R. Garcia, A. Karp, and C. Siewert, "A high-order spherical harmonics solution to the standard problem in radiative transfer," *The Astrophysical Journal*, vol. 280, pp. 853–864, 1984.

[28] I. S. Gradshteyn and I. M. Ryzhik, *Table of integrals, series, and products*. Academic press, 2014.

[29] E. Chalhoub and R. Garcia, "On the solution of azimuthally dependent transport problems with the ANISN code," *Annals of Nuclear Energy*, vol. 24, no. 13, pp. 1069–1084, 1997.

[30] E. Chalhoub and R. Garcia, "A new quadrature scheme for solving azimuthally dependent transport problems," *Transport theory and statistical physics*, vol. 27, no. 5-7, pp. 607–624, 1998.

[31] R. Garcia and C. Siewert, "Benchmark results in radiative transfer," *Transport Theory and Statistical Physics*, vol. 14, no. 4, pp. 437–483, 1985.

[32] B. D. Ganapol, "The response matrix discrete ordinates solution to the 1D radiative transfer equation," *Journal of Quantitative Spectroscopy and Radiative Transfer*, vol. 154, pp. 72–90, 2015.

[33] J. Lenoble, "Standard Procedures to Compute Atmospheric Radiative Transfer in a Scattering Atmosphere-Volume I, International Association of Meteorology and Atmospheric Physics (IAMAP)," *Boulder, Colorado, USA*, 1977.

[34] B. D. Ganapol, "Matrix riccati equation solution of the 1d radiative transfer equation," *arXiv preprint arXiv:2007.02437*, 2020.

[35] B. D. Ganapol, "1d thermal creep channel flow in the bgk approximation by adding and doubling," *Annals of Nuclear Energy*, vol. 134, pp. 441–451, 2019.

[36] B. D. Ganapol, "Particle transport in a 3d duct by adding and doubling," *Journal of Computational and Theoretical Transport*, vol. 46, no. 3, pp. 202–228, 2017.

[37] B. D. Ganapol, "Poiseuille channel flow by adding and doubling," in *AIP Conference Proceedings*, vol. 1786, p. 070009, AIP Publishing LLC, 2016.

[38] B. D. Ganapol, "A 1d radiative transfer benchmark with polarization via doubling and adding," *Journal of Quantitative Spectroscopy and Radiative Transfer*, vol. 201, pp. 236–250, 2017.

[39] E. Schiassi, C. Leake, M. De Florio, H. Johnston, R. Furfaro, and D. Mortari, "Extreme Theory of Functional Connections: A Physics-Informed Neural Network Method For Solving Parametric Differential Equations," *arXiv*, 2020.

[40] A. Previti, R. Furfaro, P. Picca, B. D. Ganapol, and D. Mostacci, "Solving radiative transfer problems in highly heterogeneous media via domain decomposition and convergence acceleration techniques," *Applied Radiation and Isotopes*, vol. 69, no. 8, pp. 1146–1150, 2011.

[41] S.-S. Chen, B.-W. Li, and Y.-S. Sun, "Chebyshev collocation spectral method for solving radiative transfer with the modified discrete ordinates formulations," *International Journal of Heat and Mass Transfer*, vol. 88, pp. 388–397, 2015.

[42] A. D. Kim and M. Moscoso, "Chebyshev spectral methods for radiative transfer," *SIAM Journal on scientific computing*, vol. 23, no. 6, pp. 2074–2094, 2002.

[43] Y.-S. Sun and B.-W. Li, "Chebyshev collocation spectral method for one-dimensional radiative heat transfer in graded index media," *International Journal of Thermal Sciences*, vol. 48, no. 4, pp. 691–698, 2009.